Journal of Fluorine Chemistry 255–256 (2022) 109964

Contents lists available at ScienceDirect

Journal of Fluorine Chemistry

journal homepage: www.elsevier.com/locate/fluor

Fluorination of two-dimensional graphene: A review

Sai Krishna Padamata [a,c,*], Andrey Yasinskiy [a,b], Srecko Stopic [b], Bernd Friedrich [b]

[a] Laboratory of Physics and Chemistry of Metallurgical Processes and Materials, Siberian Federal University, 600025 Krasnoyarsk, Russia
[b] IME Process Metallurgy and Metal Recycling, RWTH Aachen University, Germany 52056 Aachen, Intzestraße 3
[c] Department of Engineering, Reykjavik University, Menntavegur 1, 102 Reykjavik, Iceland

ARTICLE INFO

Keywords:
Fluorinated graphene
Two-dimensional material
F/C ratio
Carbon material

ABSTRACT

Fluorinated carbon materials have a wide range of applications due to their versatile properties. Functionalisation of carbon materials with fluorine enhances their properties and open their applications to new fields. Fluorinated graphene, in particular, has highly attracted researchers due to its 2-D structure, high hydrophobicity, wide bandgap and C-F bonding (ionic, semi-ionic/semi-covalent and covalent). This review gives a brief overview of the fluorination of various carbon materials such as graphite, carbon nanotubes, fullerene, and DLC and followed by an in-depth review of fluorination of 2-D graphene material. We discuss the synthetic methods of fluorinated graphene, which are mainly distinguished into exfoliation and direct fluorination. The relation between the type of bonds, F/C ratio and specific properties such as bandgap, optical properties, magnetic properties, electric and thermal conductivity and tribological properties are discussed. With a precise tuning of the F/C ratio and limiting the type of C-F bond, the fluorinated graphene can be used in battery storage devices, as a lubricant additive, as a gas sensing material and in other applications like quantum dots, supercapacitors and bioapplications.

1. Introduction

Fluorinated carbons are widely regarded as promising materials because of their properties such as excellent thermal conductivity and stability, high chemical stability, good mechanical strength, hydrophobicity [1–3]. These materials are used in energy storage systems, lubricants, and hydrophobic coatings [4–6]. In general, carbon materials are dopped with nitrogen [7–9], fluorine [10–12], phosphorous [13–15] and sulphur [16,17] between the concentration of 0 to 30 wt.% to enhance their properties which can have applications mentioned above. From the mentioned elements, fluorine has been given special attention for its chemical difference as it has high hydrophobicity, the highest electronegativity (redox potential for F_2/F^- is +2.87V) and high reactivity (due to low dissociation energy of 36 kcal/mole), among other elements in the periodic table. Furthermore, fluorine doping contributes distinct bonding and chemical abilities to carbon materials. It forms only a single bond with carbon and has more valance electrons than N, P, and S.

The type of chemical bond formed between the elements C and F and the F/C ratio depends on the kind of carbon material used, the fluorination conditions like the temperature at which the process is performed, the fluorinating agent, and the process duration. For instance, Poly(dicarbon monofluoride) $(C_2F)n$ is formed at 350°C while poly(carbon monofluoride) $(CF)_n$ at a temperature around 600°C. The higher fluorination level β (β= F: C, 0.5<β<1) of carbon compounds say $(CF)_n$ and higher covalent bond characteristics can be achieved with high reaction temperature, resulting in sp^3 hybridisation of a carbon atom [18,19]. The F/C ratio of fluorinated carbon is crucial. For instance, it has been stated in Peng et al [20]. that high F/C ratios result in the low electrical conductivity and decline in rate performance of the material due to a large number of the covalent bond. On the other hand, low F/C results in only ionic bond formation between the elements leading to the low specific capacity of the material [21].

The bond between C and F is not only limited to covalent, instead involves semi-ionic, ionic, and van der Waals interactions depending upon the type of carbon material fluorinated. Some of the carbon materials are amorphous carbon, glassy carbon, diamond-like carbon, graphite, fullerenes, and carbon nanofibers. The carbon s-p hybridisation varies among the above-mentioned carbon materials resulting in diverse electrical conductivity, electron affinity, electron ionisation potential and electric structure. There are two major fluorocarbon films structures, where Ariel et al [22]. describes the low fluorine content

* Corresponding author.
E-mail address: saip@ru.is (S.K. Padamata).

https://doi.org/10.1016/j.jfluchem.2022.109964
Received 27 October 2021; Received in revised form 13 February 2022; Accepted 16 February 2022
Available online 17 February 2022

fluorocarbon films contain irregular carbon circles as diamond-like carbon structures while the fluorine rich fluorocarbons are polymer-like with a small volume of cross-linking C-C units, C-C chains and CF_2 units [23].

Among the carbon materials, graphene and its derivatives have been given special attention since the isolation of a single layer of graphene using mechanical exfoliation by Geim and Novoselov [24]. Graphene has attractive properties such as high optical transmittance (≈ 97.7%), ultrahigh theoretical surface area (2630 $m^2 \cdot g^{-1}$), high thermal conductivity (5000 W $m^{-1} \cdot K^{-1}$) and high charge carrier mobility (200000 $cm^2\ V^{-1} \cdot s^{-1}$) [25–28]. At the same time, graphene is 200 times stronger than steel, which makes it the most robust material ever tested to date [29]. Despite all these attractive properties, the material still possesses disadvantages like zero bandgap, structural defects and chemical inertness. Micromechanical cleavage technique was used to fabricate graphene from graphite. This technique is easy to implement, producing high-quality graphene crystallites [30]. Graphene has two main derivatives, 1) Graphene oxide (GO), obtained from oxidation of graphite 2) Reduced graphene oxide (rGO), synthesised by reduction of graphite [31]. GO has various functional groups such as epoxy, carboxyl and hydroxyl group in its basal plane and carboxylic, ketone and aldehyde group on its layer edge. The presence of this functional group allows it to attach with different molecules, especially biomolecules, enhancing its mechanical and bioactivity properties, which can be used for bio-applications [32,33]. The rGO has an oxygen-containing functional group, while some defects in the structure are very similar to the pristine graphene. The surface defects and the ratio of oxygen-containing functional groups can be controlled or modified by adjusting the degree of the reduction reaction [34].

The functionalisation processes such as generating functional groups on the graphene and chemical bonding can enhance the material's properties. Fluorination of graphene can optimise the properties as it improves the chemical activity with the presence of the functional group and has tunable electrical properties such as bandgap opening and charge transfer density. The fluorinated graphene (FG) (CF_x, x = 0 to 1.12) is a nanosheet with a wide-bandgap exhibiting C-F bond characteristics from ionic, semi-ionic/semi-covalent and covalent bonds, which can be controlled by varying fluorination conditions. The FG exhibits outstanding properties such as high room-temperature resistance of over 10 GΩ and an optical bandgap of 3.8 eV [35]. In this review paper, we start by giving a brief review on the fluorination of various carbon materials (i.e. graphite, carbon nanotubes (CNTs), fullerene, and diamond-like carbon), followed by a detailed discussion of the synthesis methods, properties and applications of FG.

2. Fluorination of various carbon materials

The characteristics of fluorinated carbon mainly depend upon three main factors: the type of carbon material used, the fluorinating reagent, and the method used to synthesise the fluorinated carbon. In this section, the synthesis of fluorinated carbon materials with different carbon material types are discussed

2.1. Fluorination of graphite

Fluorinated graphite was first synthesised from the reaction between graphite and elemental fluorine at 420°C by Ruff and Bretschneider [36]. In general, fluorinated graphites (C_xF) are fluorine-graphite compounds having a semi-covalent C–F bond ($x > 2$) or a covalent C-F bond ($x \leq 2$), depending upon the synthesis conditions and fluorine content. The fine-tuning of fluorine concentration, graphite content, and C–F bonding can adjust the application properties such as tribological properties, thermal and chemical stability and the discharge potentials (stronger the C-F bond, weaker the potential) [37]. Graphite fluoride (GrF) is considered a cathode material as it has a high affinity towards lithium. However, defluorination occurs on the cathode surface due to the inevitable formation of LiF upon cycling, while the reversibility of intercalated Li-ions is possible on CF-LT (fluorinated graphite synthesised at room temperature (RT)) [38]. The material is widely used as a lubricant because of its hydrophobic nature and its weak surface interaction.

In [39], high fluorinated graphite was synthesised, where graphite was initially fluorinated with F_2 using catalysts HF and IF_5 at RT. The fluorination time was about 10 h, and the initial obtained product was in the chemical composition of $CF_{0.89}I_{0.02}H_{0.06}$(abbreviated as CF (LT)-RAW). In the re-fluorination process, the CF(LT)-RAW sample was placed in the reactor and dried for 4h in a vacuum, followed by drying in an N_2 atmosphere with 1 atm pressure for four more hours. Then the re-fluorination of the dried samples was performed between the temperatures ranging from 100 and 600°C with an interval of 50°C. A similar re-fluorination process was performed at temperatures from 150 to 600°C with an interval of 50°C on graphite fluorine ($CF_{0.47}$) obtained from the fluorination of graphite at RT with F_2 gas along with BF_3 and HF catalysts [40]. In both cases, the fluorinated graphite obtained from re-fluorination below 400°C contained minor catalysts residues and C-F bonds were a mixture of semi-ionic and covalent bonds. With refluorination at 600°C, an F/C ratio ≥ 1 was achieved, with C-F bonds being purely covalent. At temperatures from 400 to 550°C, hybrid GrF was synthesised, where the sample exhibited a double crystalline structure and had both semi-ionic and covalent C-F bonding [39]. Re-fluorination of the initial prepared product resulted in the hybridisation of the sp^2 carbon atoms into sp^3 and increased the covalent character of the C-F bonds. It is worth noting that the GrF's thermal stability increase with the rise in temperature from 100 to 600°C.

2.2. Fluorination of carbon nanotubes (CNT)

Carbon nanotubes discovery was considered a breakthrough in science and technology because of its attractive properties and a wide range of applications such as hydrogen storage, advanced composites, supercapacitor, lithium cell and secondary battery. The CNT synthesis is carried out using laser ablation, chemical vapour deposition and arc discharge [41]. The single-walled CNTs (SWNT) possess high tensile strength and can be used as insulators, semiconductors or conductors of electricity depending on their diameter and helicity. The functionalisation of CNT can improve the material properties. The bonding of the functional group with the nanotubes can improve the physio-chemical properties. The functionalisation of the nanotubes on its sidewalls results in the double bonds and hybridisation of the carbon atom to sp^3 from sp^2, where electrical, optical and mechanical properties of the nanostructural material significantly altered [42]. In the fluorination process of CNT sidewalls, no structural damage occurs. The fluorination methods mainly cover the active surface area of the nanotube, which is advantageous as it reduces further functionality of the CNT but simultaneously changes the electrical properties.

In Khabashesku et al [43]., direct fluorination was performed on SWNT prepared using the (L-SWNT) laser-ablation and (HiPco-SWNT) high-pressure C.O. disproportionation processes. The prebaked (at 1100°C) L-SWNT buckypaper was fluorinated in the range between 150 and 600°C. The IR-spectroscopy shows a C-F covalent bond for CNT fluorinated above 250°C in the absence of the HF catalyst. The fluorination above 400°C destroyed the CNT walls resulting in fluorinated graphite and some fluoro-MWNTs formation. The stable C_2F was yielded when L-SWNT was fluorinated at 350°C without any wall damage. The synthesised product just above 250°C acted as insulators (>20 MΩ). The effect of the HF catalyst was examined during the fluorination process, where the F/C ratio was 0.5. It was found that more robust and stable C-F covalent bonds were formed below the reaction temperature of 250°C. In the case of HiPco-SWNT, due to their smaller average diameter, which indicates low curvature and high reactivity, more fluorine atoms are attached to the sidewalls of the SWNT. The same strong covalent C-F bond can be achieved at fluorination temperature below

150°C. Similarly, in reference [44], when SWNT is fluorinated at 500°C or above, some of the SWNT are transformed into fluorinated MWNTs. The main reason for the appearance of MWNT when there is fluorination of SWNTs at a high temperature is because the C-C bond adjacent to the fluorine atom always breaks at high temperatures. Unlike the fluorination process of other carbon materials, the operational temperature for the fluorination of CNT requires at least 150°C to obtain completely covalent C-F bonds because of their reaction activation barrier [44].

Nakajima et al [45]. and Hamwi et al [46]. synthesised the fluorinated multi-walled carbon nanotubes (F-MWNT). It was shown in the findings that the geometry (tubular) of the MWNT did not change at fluorination temperature below 300°C. Although, fluorination temperature above 400°C resulted in cracking the outermost layer and penetration of F atoms. It is to be said that the fluorination temperature reduced to obtain F-MWNT is naturally higher compared to F-SWNT as the MWNT has multiple layers and reduce high temperature to obtain the functionality state. The MWNT can be fluorinated at RT if the HF and IF_5 are used along with the fluorine gas, and the former acts as the catalyst. The fluorination of MWNT at 500°C turned the F-MWNT to white, but when the fluorination was performed at RT with catalyst HF and IF_5, the F-MWNT remained black.

In Wang et al [47]., the MWNTs were pretreated by oxidising them before the fluorination process to obtain high F-concentration nanotubes. The MWNT with outer diameter 10-20 nm and 1-2 nm length was placed in a three-neck flask (500 mL), and 380 mL of HNO_3 was added. The solution was then stirred at 60°C for 20 h. The mixture was then washed at 120°C till the value of pH became neutral. The O concentration of this modified MWNT was at 12.5%. The fluorination process was then performed between RT and as high as 250°C. The reaction took place at the sp^3 C, which links to the oxygen-related group. The fluorine concentration in the fluorinated MWNT was as high as 9.2%. The authors stated that the process is also adaptable to other carbon materials to obtain highly fluorinated carbons.

Plasma treatment can be used to fluorinate the CNTs employing plasma gas containing fluorine, with the primary fluorination source being CF_4. The process can be performed at RT, while the fluorination only takes place on the outer layer of the nanotubes. Therefore, pollutants and byproducts are avoidable using this method. The properties of the F-CNT can be tuned by controlling the power of arc, the flow rate of the fluorine gas, and the time of the fluorination process [48]. In below Fig. 1, the dependency between the fluorine content in the CNT and the treatment time has been plotted. It can be seen that the fluorine content of the CNT increases initially until the first 30 sec, and a sudden fall occurs during the next 30 sec and remains almost the same for the next 240 sec [48]. The decrease in the fluorine content corresponds to the formation of new ionic bonds between carbon and fluorine atoms, as it states that with a substantial increase in the flow rate and time, the covalent bonds change to ionic ones.

Shoda et al [49]. and Felten et al [50]. performed fluorination of MWNTs using plasma treatment. They have stated that the MWNTs functionalisation to F-MWNT does not affect its tubular structure and C-F bonds are covalent. The chemical and physical properties can be optimised by controlling the fluorination time, fluorine gas flow and arc power.

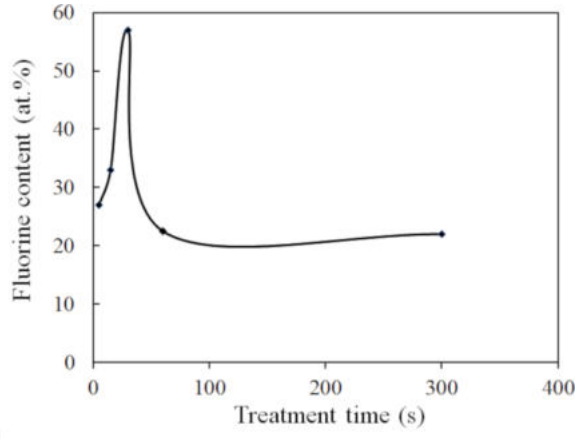

Fig. 1. The fluorine content (at.%) in the CNT vs the fluorination time using the plasma treatment.

2.3. Fluorination of fullerene

The fullerene has a unique structure that allows it to form a wide range of derivatives during its functionalisation. The high reactivity and smaller atomic size of fluorine allow multiple bonds of fluorine atom with the carbon within $C_{60}F_2$ to $C_{60}F_{60}$. Hyperfluorination (when n(F) > 60) can be achieved when the carbon sphere is ruptured, although the process requires fluorination temperature above 250°C or a strong catalyst. Below, Fig. 2 shows the presence of F atoms on the outer part of the carbon cage after the fluorination process at RT. No reaction between the fullerene and high valency inorganic metal fluorides such as BF_3 and MoF_5 took place when the latter is used as a reagent, and not a single covalent bond between C and F was observed [51]. This phenomenon is due to the low oxidising ability of these metal fluorides.

As the fluorine is highly reactive, it interacts with chemically inert fullerene molecules to form fluorofullerene. The elemental fluorine interacts with fullerene at RT, while the product formed at a temperature around 70°C is $C_{60}F_{9<x<20}$ [52]. The reaction between the fullerene and the rare earth metal fluorides was examined by Boltalina et al [53].. Due to their high oxidation states, these fluorides lose fluorine atoms quickly at the moderate reaction temperature. When fullerene (C_{60}) reacts with the TbF_4, a fluorofullerene with stoichiometry ($C_{60}F_x$ (x= 40 to 44)) was synthesised. Hyperfluorination occurred at high temperatures, where fluorofullerene$C_{60}F_{x>60}$ was produced. It was observed that an explosion occurred at the reaction temperature over 320°C, and the reaction mixture was all over the reactor.

A multilayer fullerene known as carbon nanoonions (CNO) was fluorinated by Liu et al [54].. The CNO with 50 to 100 nm diameter was transferred to a microwave reactor, sealed, and helium was pumped continuously for 2 h at RT. The temperature was then raised to the reaction temperatures (350, 410 and 480°C) and held for 3 hours to remove the moisture and air residues in and around the samples. The direct fluorination was performed with a mixture of fluorine and helium (ratio 3:1) at a fixed gas flow. The total fluorination time was 6 h, and the F-CNO with stoichiometries $C_{10.1}F$, $C_{3.3}F$ and $C_{2.3}F$ were synthesised. From the structural examination, it was established that the F-CNO still had spherical geometry like CNO. Like the other carbon materials, the F/C ratio and the covalent nature increases with the reaction temperature.

2.4. Fluorination of diamond-like Carbon (DLC)

Diamond-like carbon material has both sp^2 and sp^3 type carbon atoms, combining the characteristics of both graphite and the diamond. Fluorinated DLC has attractive properties with applications in

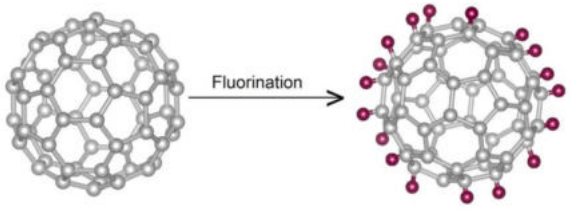

Fig. 2. Crystallographic structure of fullerene (C_{60}) to F-fullerene ($C_{60}F_{18}$) during fluorination

biosensors and biomedical implants [55–57]. DLCs are usually used as a coating to the substrate through a chemical vapour deposition method. The fluorination of DLC enhances the tribological applications of the F-DLC materials. For instance, the F-DLC has better adherence to the substrate and can improve the hydrophobic nature as the fluorine atom attached to the DLC can repel the water molecule [58].

In [59], fluorinated DLC was synthesised using the radio frequency (RF) plasma-enhanced chemical vapour deposition method on the silicon wafer. The RF of 13.56 MHz and negative electrode self-bias voltage of 400 V were parameters. Before the deposition, the silicon wafer substrate (1.5 × 1.5 cm^2) was cleaned and sonicated in isopropanol and acetone (1:1) for 5 min, followed by washing the sample with distilled water and drying under N_2 gas. The substrate was transferred to the deposition chamber placed on the water-cooled electrode driven by the radio frequency power supply. The substrate surface was further cleaned by argon gas with a flow rate of 60 $cm^3 \cdot min^{-1}$ at a chamber pressure of approximately 6.66 × 10^{-4} Pa. The CF_4 dopant was used to obtain fluorinated DLC. The film deposition was done by using an acetylene/argon mixture under plasma glow discharge. The synthesised F-DLC was further immersed in glycine solution for 6 h at a temperature around 37°C to analyse the adsorption characteristics towards the glycine and washed with distilled water. It was observed that the film density declines with a rise in fluorine dopant content. The rise in fluorine doping level resulted in a decrease in adsorption of glycine on the F-DLC, and a decrease in the F/C ratio in the film increased the adsorption levels. High fluorine content in F-DLC increased surface roughness.

In Bendavid et al [60]., F-DLC was deposited on a silicon substrate using RF-plasma-enhanced chemical vapour deposition. The fluorine content in synthesised S-DLC was up to 39.2 at.%. CF_4 and C_2H_2 mixture was used for F-DLC thin film on the substrate. With an increase in CF_4 concentration in the plasma, a linear decrease in the deposition was noticed due to the higher F^+ density. At a low fluorine concentration of about 6.5 at.%, the bonds between C-C, C-CF and C-F were observed with the help of XPS analysis. Although, at high fluorine concentrations, a peak related to CF_2 bonding was also recorded. Ion scattering spectrometry confirms that no oxygen contamination in the F-DLC and the F atoms were present on the outer surface. An increase in fluorine content in the F-DLC increased the number of CF and CF_2 bonds while the surface energy and hardness reduced. It was stated that these features contribute to the antibacterial activity of the F-DLC films.

3. Fluorination of 2D graphene

3.1. Synthesis of fluorinated graphene

3.1.1. Exfoliation method

3.1.1.1. Sonochemical exfoliation. Sonochemical exfoliation is a widely used technique capable of synthesising high-quality two-dimensional multi-layered nanomaterials. Fluorographene and single-layer fluorinated graphene can be noticed from the fluorinated graphite through ultrasonication. Gibb's free energy (ΔG) governs the intercalation process activated by the F atom, can be defined by the Eq. (1)

$$\Delta G = \Delta H - T\Delta S \quad (1)$$

Here ΔS and ΔH are the entropy and enthalpy for the interjection of solvents or the molecules. ΔH is predicted to be positive as the adjacent layers of fluorine exhibit van der Waals attraction, resulting in a positive and relatively small ΔG value. $T\Delta S$ affects the exfoliation because, at high pressure and temperature, the rise in ΔS results in ΔG decline. Therefore, FG is easily exfoliated compared to graphite [61].

A one-pot sonochemical method was used to prepare fluorographene by Gong et al [62].. Initially, fluorinated graphite with an initial concentration of 5 $mg \cdot mL^{-1}$ was added to 500 mL N-methyl-2-pyrrolidone (NMP) in a round-bottomed flask. The mixed solution was refluxed for 2 h at 60°C, followed by ultrasonication when the solution was brought to RT by cooling. The sonication was performed for as long as 100 h at an estimated exfoliation power of 32 W. The advantage of this method is that it combines the fluorographene preparation and the tuning of the F/C ratio (the F/C ratio is dependent on the time of sonication). Sun et al [63]. reported a one-pot technique for the synthesis of fluorographene in which 20 mg of fluorinated graphite powder was added to 40 mL chloroform. The mixed solution was ultrasonically treated under ambient conditions for 5 h in an icebath. The impurities in the solution were removed by centrifuging, and the resultant transparent yellow supernatant (ca. 0.1 $mg \cdot mL^{-1}$) was collected.

Microwave-assisted liquid-phase exfoliation for the preparation of high purity fluorographene was reported by Lei et al [64].. In this process, 0.125 g of fluorinated graphite was added to 25 mL of N, N-dimethyl formamide (DMF) solvent. The solution was ultrasonicated for 25 min to obtain a homogeneous slurry. The slurry was then centrifuged at 10000 rpm for 20 min to remove the excess amount of DMF. The exfoliated fluorinated graphite/DMF gel was treated for 5 min in a microwave oven with a power of 800 W. The remaining DMF gel was evaporated during the treatment, and the resultant product was high-quality fluorographene nanosheets (see Fig. 3). It was observed that there was a slight detachment of fluorine from the fluorographene at 600°C.

Preparation of fluorinated graphene using sonochemical exfoliation has advantages such as a) preparation of fluorinated graphene directly using fluorinated graphite instead of graphite, b) a simple method using nontoxic and cheap reagents for exfoliation at room temperature, c) fluorinated graphene synthesised from liquid-phase exfoliation can be further functionalised. However, it should be noted that at high-temperature exfoliations, the C−F bond weakens in fluorinated graphene leading to de-fluorination. Moreover, it is difficult to control the number of FG layers due to the weak selectivity of exfoliation.

3.1.1.2. Thermal exfoliation. The thermal exfoliation principle is based on the pressure developed from the decomposition of functional groups through thermal shocks due to rapid heating to high temperatures. FG was synthesised through rapid thermal exfoliation of fluorinated graphite by Herraiz et al [65].. The starting material being FG was synthesised by direct fluorination of Highly Oriented Pyrolytic Graphite (HOPG) at 1 atm pressure and 650°C for 6 h. The obtained covalent FG was of $(CF)_x$ structural type. The FG was exfoliated by a fast thermal shock induced by a closed silica reactor connected to an electric power

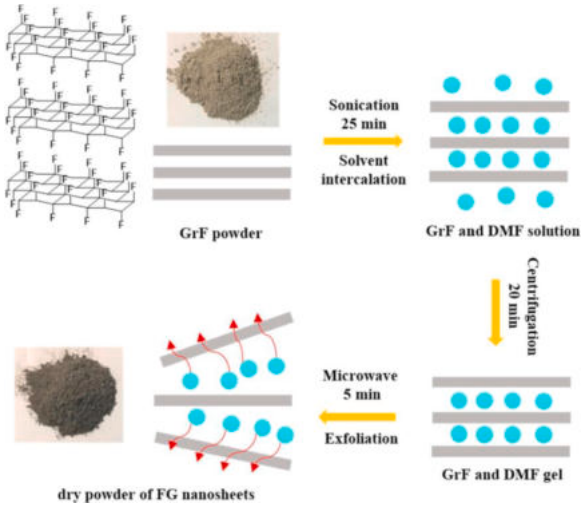

Fig. 3. Illustration of fluorographene nanosheets fabrication by solvent intercalation and microwave exfoliation. The red arrows imply the DMF solvent evaporation during microwave irradiation. Reproduced with permission [64]. Copyright 2020, Elsevier. (License no. 5177100703728)

supply. A quick temperature rise (approx. 10°C·s^{-1}) decomposes the sample, rapidly induces the generation of fluorinated gaseous species, resulting in the exfoliation of the material. The exfoliation was performed in an argon atmosphere to avoid the oxidation of exfoliated material. It was observed that exfoliation and defluorination occur simultaneously. Defluorination happens in two stages: a) from RT to 600°C, a slight decline in F/C ratio and b) rapid F/C reduction above 600°C up to 0.01. The F/C ratio was as high as 1.04 at RT. Dubois et al [66]. synthesised fluorographene by thermally exfoliating the fluorinated HOPG (prepared by direct fluorination through F_2). A sharp increase in the temperature leads to the rapid interlaminar species removal of fluorinated HOPG with a change in the colour from greyish to black, resulting in fluorographene. The specific surface area of FG increases with an increase in exfoliation temperature but at the same time drastically reduces the F/C ratio [67]. Thus by precisely tuning exfoliation temperature, C-F bonds at defects can be preferentially removed.

3.1.1.3. Electrochemical exfoliation. Fluorinated graphene can be synthesised by fluorination and exfoliation of graphite at the same time by the electrochemical method [69]. Graphite electrodes (diameter 0.5 mm), pencil rods are used as both anode and cathode material. The anode-cathode distance was 2 cm, and the applied voltage was 10 V. The hydrofluoric acid (HF) solution was used as an electrolyte with different HF concentrations (10, 20, 30, and 40 wt.%) for the electrochemical process. The studies found that the kinetics of exfoliation was very high in solutions with 20, 30 and 40 wt.% HF concentration and solution with 10 wt.% HF was considered for further studies with varying voltage and the addition of 2.5 g/L TiO_2 particles. Findings suggest that the HF electrolyte solution was incapable of synthesising multilayer graphene sheets. An increase in the applied voltage improved the exfoliation, although the fluorination degree and defect density were the highest for the powder synthesised at low voltage (2.5 V). The addition of TiO_2 in the electrolyte had a positive effect on both fluorination and exfoliation of graphite.

In another study, with the same electrode geometry and anode-cathode distance mentioned above, an electrochemical exfoliation using an electrolyte mixture of H_2SO_4 and HF with a 1:1 volume ratio was conducted [70]. Five different electrolytes were studied, 0.6 M H_2SO_4 with HF (0, 5, 10, 20, 40 wt.%). A voltage of 10 V was applied. After the electrochemical exfoliation process, the solution was ultrasonically sonicated for 45 min to improve the exfoliation efficiency. The suspension was collected and washed with deionised water three times to remove the impurities. X-ray diffraction studies showed that the lowest intensity peak was obtained for electrochemically treated powders in 0.6 M H_2SO_4 (HF 0 wt.%).

In comparison, the highest was obtained in an electrolyte mixture of 0.6 M H_2SO_4 and 40 wt.% HF. The volume of graphene layers increased with a rise in the HF concentration in the electrolyte from 0 to 5 wt.%. However, it was noted that further increase in the HF concentration led to not-exfoliated graphite with the presence of fluoride compounds and an increase in the defect density of the exfoliated powder. Raman spectroscopy confirms the successful synthesis of FG through the electrochemical exfoliation method.

3.1.1.4. Mechanical exfoliation. Ball milling assisted exfoliation of GrF in preparing graphene fluoride was performed by Vu et al [71]., as shown in Fig. 4. A GrF (5 g) with a 200–500 nm average lateral size was initially added to a 100 mL NMP solvent. The mixture was transferred to the grinding bowl (500 mL) followed by the addition of zirconia balls of 2 kg with diameters of 2 mm and 0.2 mm with a mass ratio of 1:1 to the grinding bowl. The milling was performed at 300 rpm under a nitrogen atmosphere at RT for 6 h. After the milling process, the solution was removed from the grinding bowl and centrifuged for 30 min at 2000 rpm for the removal of unexfoliated GrF. The supernatant was collected, filtered and washed with NMP. The solution was then filtered through a 0.1 μm nylon membrane filter. The exfoliated graphene fluoride (EGF) powder was acquired after two days of freeze-drying the filtered solution. The EGF's average lateral size was 800 nm. The obtained EGF powder weighed 1.9 g, which corresponds to a yield of 38%, indicating a great potential to implement this method on a large scale.

Wan and Ma [72] performed an ammonia carbonate assisted ball milling process on GrF for the exfoliation of functionalisation fluorinated graphene sheets (FFGS). GrF powder with an F content of about 56 at.% was used in this process. 1 g of GrF is added to 4 g of ammonia carbonate and mixed by hand in a beaker. The mixture was transferred to a ball milling jar of 50 mL, and 120 agate balls with 6 mm diameter were added. The mixture is milled for 20 h at 400 rpm. To avoid the agglomeration of the mixture, the jar was periodically paused, and the edges of the jar were agitated to increase the milling efficiency. After the ball milling, a grey-black mixture was attained. The obtained product was then washed 2–3 times with deionised water, followed by sonication in deionised water for 30 min and left for 1 h. Finally, the sediment was removed, filtered and dried in a vacuum oven at 60°C. The obtained final product was FFGS. The thickness of the FFGS monolayer was between 0.67 and 0.87 nm. The fluorine concentration in the FFGS was 30 at.% which is less compared to that of GrF. It was also observed that a significant amount of nitrogen and oxygen (12 at.%) was present. The main advantage of using the ball milling process would be the easy preparation of multi-layer fluorinated graphene sheets. However, the lamellar structure of graphene is damaged during the process, exposing the edge of the fractured surface. This newly available active area is preferentially fluorinated by the fluorine source resulting in edge-functionalised graphene.

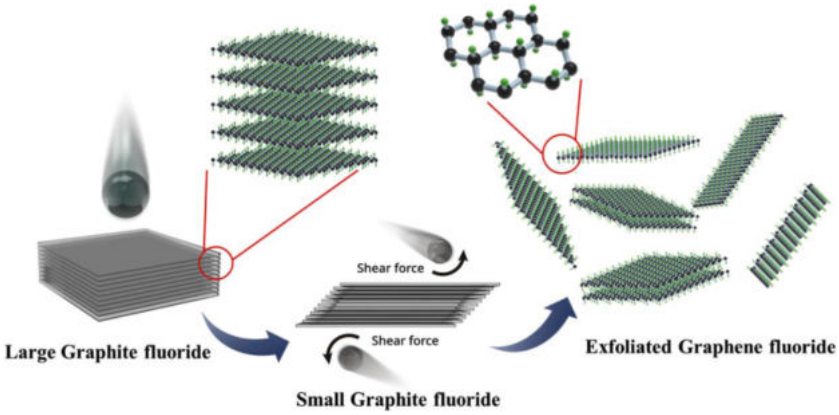

Fig. 4. An illustration of ball milling assisted exfoliation of FG. Reproduced with permission [71]. Copyright 2020, Elsevier. (License no. 5177100564613)

3.1.2. Fluorination method

3.1.2.1. Direct gas fluorination. Bi et al [73]. synthesised fluorinated graphene material using a direct gas fluorination technique. Hummer's method was used to prepare the graphene oxide (a base material to synthesise FG) from natural flake graphite. A mixture of 5 mL GO (concentration of 5 mg·mL^{-1}) and 20 μL ethylenediamine (EDA) was heated at 60°C in a Teflon reactor for 6 h to obtain reduced graphene oxide aerogel. To synthesise FG, reduced graphene oxide aerogel was further heated under N_2 atmosphere to a required temperature (between 200 and 350°C) at the rate of 2°C min^{-1} in a monel alloy tube. A mixture of N_2 and F_2 (with 10 vol.% F_2) gases was pumped into the tube and left for 1 h. Excess/residual F_2 was removed from the reactor by introducing N_2 gas after the fluorination process. The deionised water was used to wash the FG to remove the unbonded F atoms, then dry the samples in a vacuum. Fig. 5 gives a schematic representation of the direct gas fluorination method. It has been noted that with an increase in the fluorination temperature, the F/C ratio increased, followed by a significant drop. This phenomenon is due to the decomposition of C-F bonds at high temperatures, which leads to the transformation of sp^3 carbon to sp^2.

Synthesis of fluorinated graphene at room temperature would reserve most original fluorine atoms. Fluorinated graphene with a high F/C ratio (≈ 0.67) was prepared using porous graphene at room temperature by direct F_2 gas fluorination. Low process temperature and high activation effect of direct fluorination during the preparation of fluorinated porous graphene is attributed to the defect structure (meso and microporous structure) of the porous graphene [74]. Moreover, the specific surface area of fluorinated porous graphene is around 1200 $m^2 \cdot g^{-1}$, which is above the theoretical value of fluorinated graphene sheets (1018 $m^2 \cdot g^{-1}$). FG synthesised using direct fluorination contain radical fluorine atoms which are stable in the air atmosphere. The radicals can be regulated by controlling the degree of fluorination. For instance, the fluorinated graphene with low or high F/C ratios contains low fluorine radical atoms, while moderately fluorinated graphene (F/C = 0.4 – 0.5) has a high radical density [75].

3.1.2.2. Plasma fluorination. Plasma fluorination is a relatively easy, clean and safe technique to synthesise fluorinated graphene. In this method, an electron beam is projected on a targeted material, leading to the generation of fluorine radicals adsorbed on the graphene surface, leading to various C-F bonds. Plasma sources such as F_2, SF_6 and CF_4 are being used for fluorination. Hui et al [76]. synthesised a single layer FG by controlled SF_6 plasma treatment, and the maximum fluorine content achieved was ≈ 24.6 at.% for 20 s plasma treatment. A comparative study was conducted on fluorination of graphene with SF_6 and CF_4 gases through plasma fluorination by Struzzi et al [77].. Tectra plasma source with ion accelerations of 0 and 1 kV was used for the fluorination process. The plasma treatment at 1 kV was performed for 10 min (for both the gases), although the fluorination time varied at 0 kV, which was 20 min and 35 min for SF_6 and CF_4, respectively. Fluorine content on the samples treated with SF_6 plasma was 10 and 8 at.% at 0 and 1 kV, respectively, while the samples treated with CF_4 plasma were 10 and 6 at.% at 0 and 1 kV, respectively. The samples treated with SF_6 plasma had better fluorination coverage compared to the CF_4 plasma source. The sulfur atoms from the SF_6 plasma sources bonded with the copper area without affecting the surface of the graphene unless there is a restriction of the ion's kinetic energy.

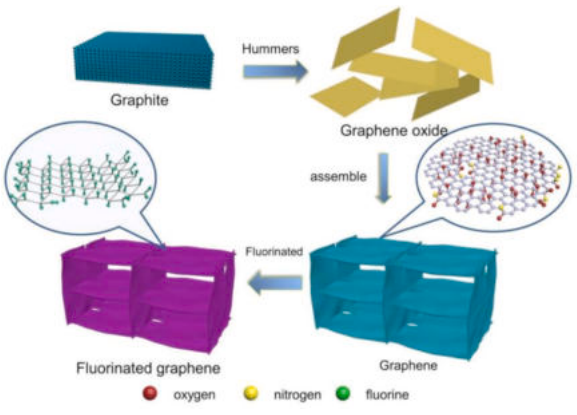

Fig. 5. Schematic for the direct fluorination method for the synthesis of fluorinated graphene. Reprinted with permission from [73] without changes under the Creative Commons Attribution 4.0 International License (http://creativecommons.org/licenses/by/4.0/)

Plsek et al [78]. synthesised fluorinated graphene employing a novel laser-ablation-assisted plasma fluorination method using an SF_6 fluorination source (Fig. 6). Initially, graphene was synthesised using the chemical vapour deposition method on copper foil. The graphene on copper foil was assembled to a sample holder in a vacuum chamber (15 cm^3) made from a conflat CF 40 viewpoint and a CF 40 to KF 16 adapter flange, which can be closed using an angle valve. The chamber was initially turned into a vacuum followed by SF_6 pumping at a pressure of $\approx 7 \times 10^{-1}$ mbar. An Nd: YAG laser beam was focused on the silicon target. The laser spot was placed 3 mm apart from the sample plane, and they are perpendicular to each other (Fig. 6). CF, CF_2 and CF_3 species were identified on the fluorinated samples. Sulphur was found on samples with low fluorine coverages. The fluorine content decreases when the number of laser pulses is higher than the saturation values. This technique can control the fluorination of the samples by controlling the applied laser pulses. The maximum fluorine atomic concentration was 60% in this method which is high compared to traditional plasma methods.

High-density plasma is required to synthesise fluorinated graphene with a high F/C ratio as the fluorine radicals energies are higher than the energies of fluorine-containing ions (CF_3^+, CF_4^+, F^-). A severe ion bombardment at high reaction temperatures leads to the carbon structure damage of graphene [79]. Moreover, plasma fluorination requires process optimisation to produce fluorinated graphene at a larger scale. As the process requires expensive setup and fluorine coverage on graphene is limited to the plasma-treated area.

3.2. C-F bonding characteristics

C-F bonding characteristics mainly includes the C-F bonds and F/C ratio of fluorinated graphene. Control over the F/C ratio is essential in opening the bandgap, tuning optical transparency, electrical conductivity, and other properties like thermal and magnetic. The fluorination conditions, treatment time, fluorinating agent, type of carbon used, and treated sides tune the F/C ratio of the FG. For example, Yu et al [80]. reported that the F/C ratio (0.17 – 0.27) of the fluorinated graphene oxide (FGO) depends on the exposure time of CF_4 plasma. Wang et al [81]. prepared highly fluorinated graphene from graphene oxide using

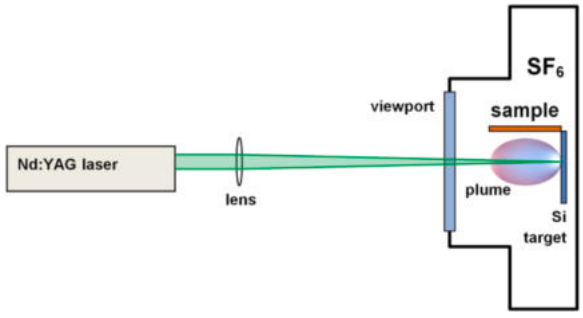

Fig. 6. Schematic diagram of laser ablation of Si target in an SF_6 atmosphere for graphene fluorination. Reproduced with permission [78]. Copyright 2020, Elsevier. (License no. 5177100405933)

direct heating fluorination. The F/C ratio increases from 0.65 to 1.02, increasing the F_2 gas concentration (from 2% to 10%) in the F_2/N_2 gas mixture at 180°C. With an increase in the operating temperature to 250°C, the F/C ratio of 1 can be achieved at 5% F_2 concentration. The composition of main C-F-containing groups (C_{sp2}-F, C_{sp3}-F, CF_2, CF_3) depends on the reaction temperature and F_2 concentration; the C_{sp2}-F (sp_2 hybridised C atoms connected to F) composition decreases with an increase in the F_2 concentration during the treatment [81]. Meduri et al [82]. reported that the F/C ratio (0.47 – 0.89) of FG increases with operating temperature (25°C – 150°C) in the direct fluorination method. At high F/C ratios, the insulating surface groups CF_2 and CF_3 are dominant. The studies suggest that a decrease in the F/C ratio results in hyperconjugation, which occurs due to the coexistence of C-F bonds and sp^2 nonfluorinated carbon atoms due to poor fluorine coverage [83]. The hyperconjugation reduces the C-F bonding order, resulting in the weakening of C-F covalence [84].

In a study by Wang et al [85]., fluorination of graphene oxide with F_2/N_2 mixture was performed, where the F/C ratio increased with an increase in the fluorination temperature, as shown in Fig. 7**a**. A rapid increase in the F/C ratio can be seen between temperatures 180 and 220°C. Fig. 7**b** shows the evolution of the band of C-F as a function of the F/C ratio. Fourier transform infrared spectroscopy (FTIS) shows a band composed of two peaks at 1150 cm^{-1} and 1220 cm^{-1}. The peak at 1150 cm^{-1} is dominant at a low F/C ratio. While the peak at 1220 cm^{-1} gains prominence with an increase in the F/C ratio. C-F bonding is differentiated based on the type of C hybridisation linked with the F atom. The peak at 1220 cm^{-1} corresponds to the C_{sp3}-F covalent bond, and the peak at 1150 cm^{-1} is the C_{sp2}-F semi-ionic (semi-covalent) bond. The C_{sp3}-F are linked at the strongly deformed carbon framework with an F/C ratio of 1, while the C_{sp2}-F bonds are present at weakly fluorinated regions (F/C $\leq$ 0.5). Gong et al [86]. reported that the FTIR spectra of photochemically synthesised FG show the semi-ionic and covalent C-F bond absorption peaks at 1151 cm^{-1} and 1212 cm^{-1}, respectively. The C-F_2 (292.2 eV) and C-F_3 (293.4 eV) groups were found in XPS studies, indicating that the sample has a high degree of fluorination. The average height within 0.9 to 1.5 nm was found for fluorinated graphene sheets, corresponding to single and double-layer sheets [86]. Ultraviolet irradiation of FG in toluene results in a rapid decrease of F/C ratio with irradiation time. The covalent C-F bonds are converted into semi-ionic C-F bonds as covalent bonds are sensitive to ultraviolet [87].

Weakening of covalent nature between the C and F atoms would lead to increased new functional groups. In comparison to GO, FG is highly reactive to ammonia. For instance, defluorination occurs when FG comes in contact with ammonia and leads to N-doping in significant degrees. C-F bonds are replaced with C-NH_2 groups. Dissociation of C-F bond facilitates dissociating of C-C and formation of C-N bond [88]. Table 1 summarizes the methods and reagents used to fabricate fluorinated graphene and their influence on the F/C ratio and C-F characteristics of fluorinated graphene.

4. Properties

4.1. Bandgap

Graphene exhibits unique electric properties due to its high carrier mobility and zero bandgap, showing good potential for advanced electronic applications. However, the zero band gap of graphene leads to high power dissipation and leakage of currents, regulating its application in standard logic circuits as a candidate of post-silicon electronics [89]. Therefore, opening the bandgap of graphene through structural engineering is highly desired. For instance, a wide bandgap of 3.1 eV opens for fluorinated graphene due to the trigonal sp^2 carbon structure transformation to tetragonal sp^3 [90,91]. Wang et al [92]. prepared fluorinated graphene sheets (FGS) through a hydrothermal reaction between HF reagent and graphene oxide. The fluorine coverage of graphene can be controlled by varying the reaction time, temperature, and HF content. The bandgap of FGS increases with an increase in fluorine coverage, where $CF_{0.09}$ has a bandgap of 1.82 eV, and $CF_{0.325}$ has 2.99 eV. This is due to the interaction of p orbits of F with π orbits of C, resulting in the change in charge densities.

According to the density functional calculations, varying FG's layers and structural configurations can control the bandgap. A chair configuration has a bandgap of 3.036 eV, while the bandgap for boat and tricycle configurations are 2.503 eV and 3.247 eV, respectively [93]. Low bandgap in boat configuration is due to a greater C-C bond length caused by F-F repulsion. The C-C bond length of chair, boat and tricycle

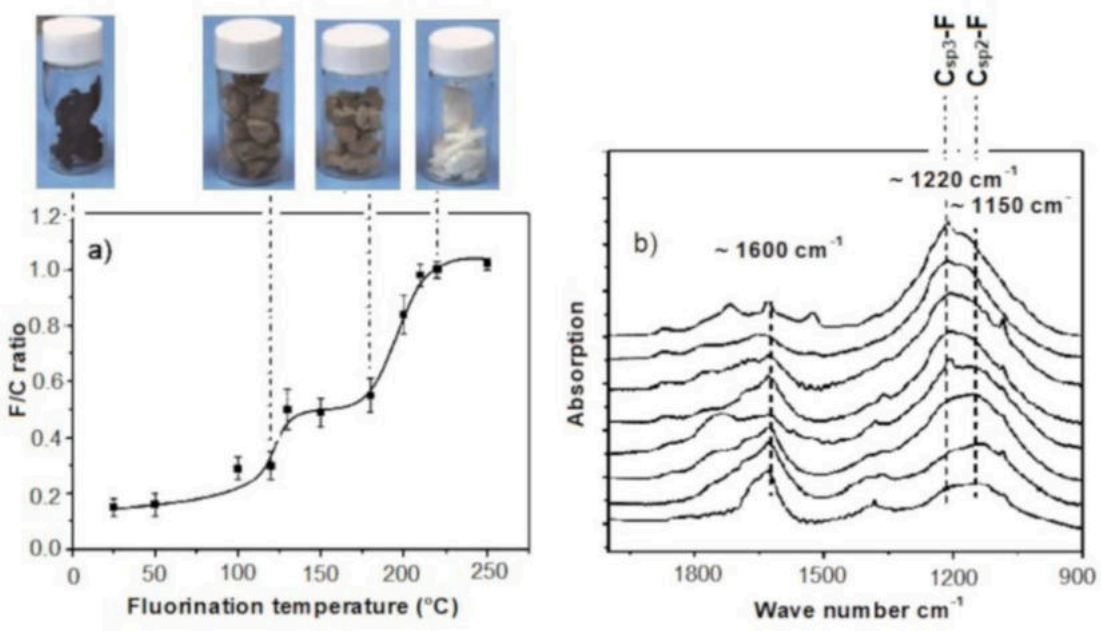

Fig. 7. a) Change of F/C ratio during the fluorination of graphene oxide with F_2/N_2 mixture b) Evolution of FTIR spectra of fluorinated samples with fluorinating temperatures (bottom to top: 50, 100, 120, 130, 150, 180, 200, and 220°C). (Reproduced/adapted with permission from ref [85], Copyright, 2016, American Chemical Society).

Table 1
Synthesis methods used for the fabrication of fluorinated graphene and their influence on C-F characteristics.

Method	Raw materials		Reaction temperature	F/C ratio	Peak location in FTIR (cm^{-1})		Peak location in XPS (eV)		Ref.
	Graphene-based materials	Fluorination source			Semi-ionic C-F	Covalent C-F	Semi-ionic C-F	Covalent C-F	
Sonochemical exfoliation	Fluorinated graphite	N-methyl-2-pyrrolidone	Room temperature	0.31–0.78	1084	1212	F1s 688.5	F1s 689.0	[62]
Sonochemical exfoliation	Graphite fluoride	N, N-dimethyl formamide	Room temperature	0.89–0.94	-	1216	C1s 284.8	C1s 285.3	[64]
Thermal exfoliation	Fluorinated graphite	F_2	650°C	0.01–1.06	1120	1199	-	-	[65]
Thermal exfoliation	FGO		400–800°C	0.057–0.16	-	-	C1s 288.4	C1s 290.3	[68]
Electrochemical exfoliation	Graphite	HF solution	Room temperature	0.046	-	1280	-	-	[69]
Mechanical exfoliation	Graphite fluoride	N-methyl-2-pyrrolidone	60°C	0.69–0.85	-	-	F1s 687.8	F1s 688.2	[71]
Direct gas fluorination	Graphene oxide	F_2/N_2 mixture	200–350°C	0.43–0.67	-	1226	F1s 687.5	F1s 688.6	[73]
Plasma fluorination	Graphene	SF_6	Room temperature	0.32				F1s 688.6	[76]

configurations are closer to the diamond bond length of 1.52 Å (sp^3 hybridisation). In-chair configuration, fluorine atoms bond with the graphene plane above and below. Khatami et al [94]. used the first principle method to study the electrons and holes phonon-limited mobility in hydrogenated graphene and fluorinated graphene. At an extreme cut-off for long-wavelength out-of-plane acoustic (ZA) phonons, electron and hole mobilities of 28 and 41 $cm^2 \cdot V^{-1} \cdot s^{-1}$ for hydrogenated graphene and electron and hole mobilities of 96 and 30 $cm^2\ V^{-1}\ s^{-1}$ for FG were obtained, respectively. However, at a more favourable cut-off wavelength ~2.6 nm, high electron mobility of 233 $cm^2\ V^{-1} \cdot s^{-1}$ and hole mobility of 389 $cm^2 \cdot V^{-1} \cdot s^{-1}$ for graphane and electron mobility of 460 $cm^2 \cdot V^{-1} \cdot s^{-1}$ and hole mobility of 105 $cm^2 \cdot V^{-1} \cdot s^{-1}$ for FG were achieved, respectively. At the same time, a complete suppression of ZA phonons increased the electron and hole mobility in graphane up to 278 and 391$cm^2 \cdot V^{-1} \cdot s^{-1}$, respectively. Meanwhile, it affects the carrier mobilities in FG. The electron transport property of FG is correlated to the fluorine distribution on the graphene surface (at low fluorine content). At the same fluorine concentrations, different island and chain-like clusters are formed on the graphene, influenced by the fluorination probability of a C atom [95].

4.2. Optical properties

A drastic change in optical properties of graphene, such as absorption band, transparency, and photoluminescence, occurs when it is functionalised with fluorine. The optical transparency of FG synthesised using XeF_2 fluorinating agent at 70°C was investigated by Nair et al [96].. As shown in Fig. 8**a**, graphene's opacity peaks at 4.6 eV and absorption intensity are not linear after the energy ~2.5 eV, which was following pronounced von Hove similarity. Partially fluorinated graphene has relatively higher transparency compared to pristine graphene. Fluorographene remains fully transparent for light energy ≤ 3 eV but starts absorbing violet lights. This implies that fluorographene is a wide-gap semiconductor with an energy gap greater than 3 eV. Robinson et al [35]. reported that graphene films treated with XeF_2 gas at 30°C exhibit optical transparency. Figs. 8**b, A** and **B** show the optical micrograph of graphene before and after one-sided fluorination, and optical contrast upon fluorination is visible between them. Fig. 8**b(C)** shows that the absorption peak related to single-layer graphene disappears but not for bilayer graphene, which indicates that fluorine chemisorption occurs only on the top surface and does not intercalate between the layers. Fig. 8**b(D)** shows partially FG, where small portions of the C_4F were not completely transparent.

Mubarak and Ismail [97] investigated the optical properties of FGS

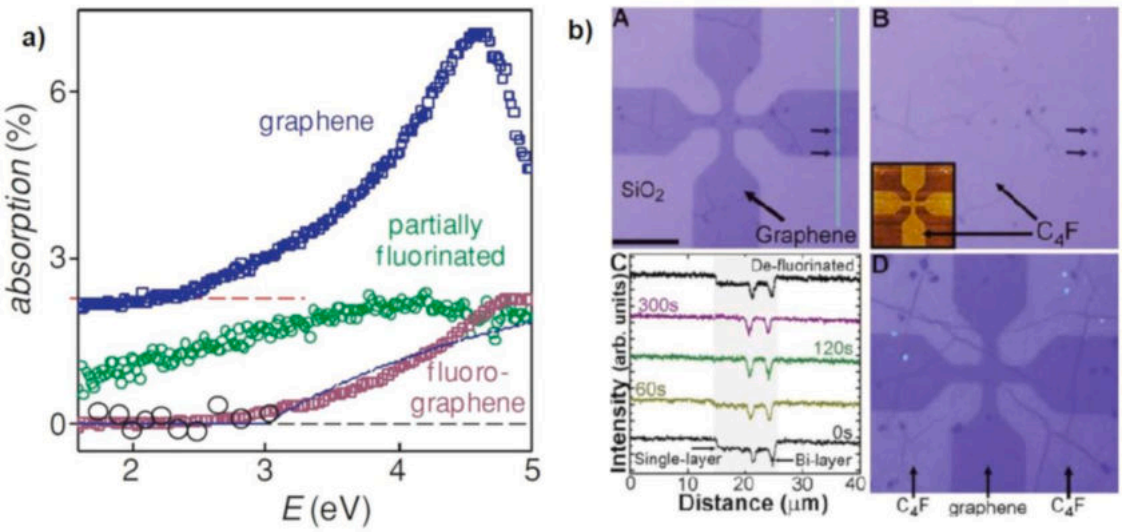

Fig. 8. a) Optical transparency changes in graphene after the fluorination process. The absorption spectra of fluorographene (bottom), partially fluorinated one (middle) and pristine graphene (top curve). Reproduced with permission [96], Copyright 2010, John Wiley and sons. (License no. 5177100033311) b) Optical characteristic changes of graphene upon fluorination on a single side. Reproduced with permission [35], Copyright 2010, American Chemical Society.

using ab initio studies. The absorption coefficient (I_w) of FGS was 121.6 $\times 10^4 \cdot cm^{-1}$, relatively low compared to the I_w of pure graphene sheets (GS) (189.9 $\times 10^4 \cdot cm^{-1}$). The optical conductivity ($\sigma(\omega)$) of FGS (3.32 $\times 10^3 \cdot \omega^{-1} \cdot cm^{-1}$) is low compared to pure GS (5.35 $\times 10^3 \cdot \omega^{-1} \cdot cm^{-1}$) which indicates that the transparency of graphene increases with fluorination. Both I_w and $\sigma(\omega)$ highest values were found in the energy levels of 14.6 – 15.0 eV.

4.3. Magnetic properties

The graphene exfoliated from highly oriented pyrolytic graphite exhibits diamagnetic behaviour with no resemblance of ferromagnetism were observed [98]. In some cases, the ferromagnetic nature of graphene is due to the localised unpair spins caused by the point defects and edge states [99]. Fluorination of graphene drastically changes the magnetic behaviour of the graphene material. Nair et al [100]. reported that the paramagnetism of FG increases with the F/C ratio (0 to 1), which the Brillouin function can precisely define:

$$M = NgJ\mu_B \left[\frac{2J+1}{2J}\ \mathrm{ctnh}\left(\frac{(2J+1)z}{2J}\right) - \frac{1}{2J}\mathrm{ctnh}\left(\frac{z}{2J}\right)\right] \quad (2)$$

where $z = gJ\mu_B H/k_B T$, N is the number of spins, k_B is the Boltzmann constant, g is the g-factor, and J is the angular momentum number. The Brillouin function provides a good fit only if $J = S = ½$ (free-electron spin). However, the magnetisation curves are best fitted at $J = 0.83$ for fluorinated reduced graphene oxide (FRGO) [101]. The FRGO (F/C ratio = 0.46) shows strong paramagnetism, suggesting the presence of high-density unpaired spins.

Wang and Li [102] conducted a theoretical study to understand the effect of charge doping on the magnetic properties of FG. Without charge (not doped), the FG has a magnetic moment of 0.72 μ_B. The fluorinated graphene continuously increases its spin moment with the variation in charge (towards positive) and obtains up to 1.08 μ_B with a positive charge of 0.6e. At the same time, magnetism changes from ferromagnetism to non-magnetism when it achieves a negative charge greater than -0.6e. Feng et al [103]. reported that the high-intensity magnetic moments are found in annealed FGO due to the improved edge effect of small fluorine clusters. These small F clusters are formed by the fragmentation of large F domains, attributed to the magnetic ordering in FG because of the shrunken average spacing between the localised moments. Thus, annealed fluorinated graphene samples can undergo the transaction from paramagnetism to ferromagnetism.

4.4. Electronic conductivity

The single-layer graphene exhibits high electron mobility due to the formation of an π–conjugated bond by the sp^2 hybridised C atom with a p_z orbital. Meanwhile, fluorination of graphene (controlled F/C ratio) can modify the electronic conductivity by transforming its metallic/semiconductor behaviour into the insulator with the retreatment of the π–conjugated bond. Fan et al [104]. reported that the electrical conductivity of GS is as high as 20200 $S \cdot m^{-1}$ after annealing. The electrical conductivity of graphene can be significantly reduced with the increment of the F/C ratio, and electrical conductivity of as low as 2 $S \cdot m^{-1}$ can be achieved at an F/C ratio of 0.5 [92]. The resistance of FG is greater than 7 orders in magnitude compared to pristine graphene, where the resistance of FG is around 1 TΩ with fluorine coverage of a few tenths of a percent [105]. At a very low F/C ratio, the FG behaves as a semiconductor due to the existence of sp^2 hybridised C atoms [106].

Kolesnik-Gray et al [107]. reported that the electrical conductivity of the fluorinated graphene also depends upon material geometry. The studies were conducted on fluorinated graphene thin films and flakes. In the case of graphene films, the electrical conductivity decrease by five orders of magnitude with fluorination (F content from 2.4 to 14.6 at.%). In contrast, the electrical conductivity of graphene flakes increases by a magnitude of two orders with fluorination (2.4 to 16.6 at.%). This phenomenon is because the edges of the flakes are the primary sites of fluorine, making them behave like unfunctionalised graphene. The covalently attached fluorine on the flakes preserves its electrical properties. Also, the charge transport in thin-film FG is affected by the edge/edge, edge/plane, and plane/plane junctions [108].

4.5. Thermal conductivity

Graphene possesses high thermal conductivity of 5300 $W \cdot m^{-1} \cdot K^{-1}$ due to efficient phonon transfer by ion-core vibration in the crystal lattice [109,110]. However, the high electrical conductivity of graphene restains its applications in highly coherent electronic devices. By fluorination of graphene, high electrical insulation and high thermal conductivity can be achieved. Ultrathin graphene fluoride films were synthesised from the graphene fluoride solution prepared by mechanical exfoliation of GrF. The films exhibit an excellent in-plane thermal conductivity of 242 $W \cdot m^{-1} \cdot K^{-1}$ and incredible through-plane thermal conductivity of 21.8 $W \cdot m^{-1} \cdot K^{-1}$ at 10 mm thickness with electrical conductivity of $>10^{-12}$ $S \cdot m^{-1}$ exhibiting excellent flexibility. The thermal conductivity can be tuned by altering the thickness of the film [71]. A graphene fluoride- poly (vinyl alcohol) composite suspension was prepared from sonochemically exfoliated graphene fluoride and poly (vinyl alcohol) via vacuum filtration. The film prepared by this suspension has an ultrahigh in-plane thermal conductivity of 61.3 $W \cdot m^{-1} \cdot K^{-1}$ at 93 wt.% graphene fluoride [111]. A non-equilibrium molecular dynamics (NEMD) study was conducted to estimate the theoretical thermal conductivity of FG [112]. The thermal conductivity decreases rapidly when Fluorine coverage increases between 0% and 20%, normalises from 20% to 70% and quickly increases when approached 100%.

4.6. Tribological properties

Graphene possesses good tribological properties due to its chemically inert behaviour, surface adherence, low shear strength, and characteristics of lamellar structure [113,114]. The fluorination of graphene can enhance its tribological properties. Hou et al [115]. reported that fluorinated graphene significantly reduces the wear volume and friction coefficient as an oil-based lubricant additive. Fluorographene as a lubricant additive can reduce friction because of the low interlayer interaction caused by the repulsive electrostatic forces between the F atoms at the interfaces [116]. The wetting contact angle of FG is much larger compared to that of the angle measured on the pristine graphene surface, suggesting that the FG has a more hydrophobic surface [117, 118]. Molecular dynamics simulation reveals that the high hydrophobicity of fluorinated graphene is due to its low interfacial density and high water slip length, while graphene has high interfacial density and low slip length, meaning it shows low hydrophobicity [119]. The nanoscale friction of the graphene after fluorination increases six times, as shown in Fig. 9. Meanwhile, after fluorination, the adhesion force is reduced to about 25%, i.e. from 44 ± 10 nN (for pristine graphene) to 32 ± 10 nN (for fluorinated graphene) [120]. The tribological properties of FG mainly depend on its surface chemistry (species attached on its surface), F/C ratio and microstructure (such as interlayer spacing and interlayer interaction, F atoms arrangement) [115]. Table 2 compares the properties of pristine graphene and fluorinated graphene discussed in this section.

5. Applications

5.1. Energy Storage Devices

Watanabe and Fukuda [122,123] were the first to use fluorinated carbon (CF_x) as a cathode material in lithium primary batteries (LPBs). CF_x was considered a promising cathode material for LPBs due to its

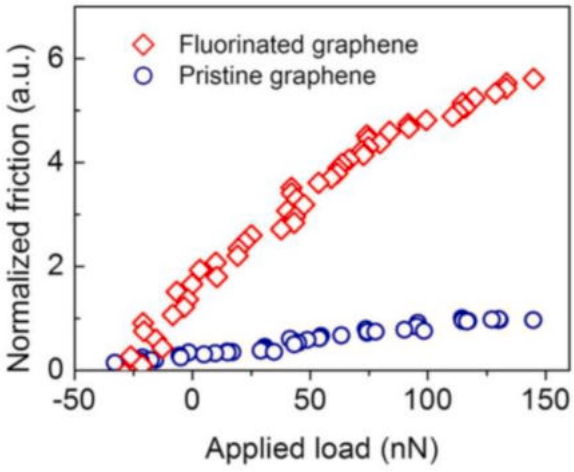

Fig. 9. Friction force vs Applied load recorded on fluorinated and pristine graphene. Reproduced with permission [120], Copyright 2010, American Chemical Society.

Table 2
Comparing the properties of graphene and fluorinated graphene material.

Properties	Graphene-based	Fluorinated graphene-based	Ref.
Bandgap	0 eV	3.8 eV	[91,92]
Electron mobility	233 $cm^2 \cdot V^{-1} \cdot s^{-1}$	460 $cm^2 \cdot V^{-1} \cdot s^{-1}$	[94]
Optical conductivity	5.35 × $10^3 \cdot \omega^{-1} \cdot cm^{-1}$	3.32 × $10^3 \cdot \omega^{-1} \cdot cm^{-1}$	[97]
Electrical conductivity	20200 $S \cdot m^{-1}$	2 $S \cdot m^{-1}$	[92, 105]
Adhesion force	44 ± 10 nN	32 ± 10 nN	[120]
Coefficient of friction	0.17	0.08	[121]

stable operation ability, wide operating temperature, high energy density, and high average operating voltage. A very high theoretical energy density of 2180 $Wh \cdot kg^{-1}$ is possessed by CF_x (for graphite at x =1) as cathode material for LPBs. Fluorinated mesoporous carbon ($CF_{0.54}$) exhibited excellent performance with a 515 $mAh \cdot g^{-1}$ capacity and a discharge plateau of 2.75 V at a current rate of 5 C [18]. But the power densities are not satisfactory because of the poor electrical conductivity possessed by fluorinated carbon from strong C-F covalent bonds.

Damien et al. reported that LPBs utilising fluorinated graphene with low fluorine content (x = 0.22) exhibits excellent electrochemical performance [124]. The specific capacity of FG was 767 $mAh \cdot g^{-1}$ at 10 $mA \cdot g^{-1}$ current density, which is greater than the specific capacity of fluorinated graphite polymer $(CF_{0.25})_n$, which is 550 $mAh \cdot g^{-1}$ at a similar current density. The faradic yield of the FG was 210% at 10 $mA \cdot g^{-1}$. The specific capacity of FG and fluorinated graphite polymer at a very high current density of 1000 $mA \cdot g^{-1}$ was 572 $mAh \cdot g^{-1}$ and 408 $mAh \cdot g^{-1}$, respectively. FG (F/C = 0.8) prepared by one-step gas fluorination of rGO possesses an excellent power density of 21460 $W \cdot kg^{-1}$ and a very high energy density of 1073 $Wh \cdot kg^{-1}$ at a current density of 10 $A \cdot g^{-1}$ [125]. Sun et al [126]. reported that LPBs with FG electrodes exhibited an excellent discharge rate due to higher charge mobility with good Li^+ diffusion through the nanosheets. FG containing semi-ionic F-C bonds with a specific capacity up to 520 $mAh \cdot g^{-1}$ at a current density of 1 C, five times higher than the specific capacity of fluorinated graphite [126]. FG also has a 4038 $W \cdot kg^{-1}$ power density at 3 C, four times higher than fluorinated graphite [126]. LPBs with fluorinated graphene microspheres (FGM) have a record cell-level power density of 12451.2 $W \cdot kg^{-1}$ at 20 C. Moreover, FGM (F/C = 1.03) cathodes have high active material mass loading (4.3 $mg \cdot cm^{-2}$) and perform excellently in extreme operating temperatures (up to 100°C) [127].

Jeon et al., for the first time, synthesised edge-selective fluorinated graphene nanoplatelets (FGnPs) through the mechanochemical ball-milling method, which can be used as a cathode on lithium-ion batteries (LIB). The FGnPs showed excellent stability and cycle life, with 650.3 $mAh \cdot g^{-1}$ specific capacity at a current rate of 0.5 C, with 76.6% charge retention after 500 cycles [128]. Chen et al. theoretically studied Li adsorption, diffusion, and storage mechanism on single-sided FG via density functional theory simulation. FG (F/C=0.5) exhibits a very low lithium-ion diffusion barrier (0.04 eV), maximum lithium storage capacity of 623 $mAh \cdot g^{-1}$ and high open-circuit voltage of 0.96 V [129].

Liu et al [130]. introduced FG in sodium batteries with a good performance rate but a large voltage gap between the charge and discharge process. The initial discharge capacity for Na/CF_x battery was 840 $mAh \cdot g^{-1}$ at 0.025 C with a polarisation of about 1200 mV. The addition of Ag nanoparticles to the FG substantially reduced the cell voltage by 480 mV, resulting in low overpotential and high electric efficiency. Thus, the addition of Ag nanoparticles to FG improved the performance of the Na/CF_x battery [130].

5.2. Lubrication

Graphene-based additives have been extensively used in lubricants, as the additives improve the load-carrying capacity, anti-oxidation and anti-wear ability of the lubricants and provide a low coefficient of friction [131–133]. Meanwhile, the addition of FG into the lubricant only enhances its properties. For instance, the addition of fluorographene to polyimide (PI) can effectively improve the anti-wear performance of the PI [134]. The PI and PI/fluorographene nanocomposites coating were tested under dry sliding conditions. The worn surface of the PI and PI/fluorographene nanocomposite exhibits severe plastic deformation and microcracks, as shown in Fig. 10 **(a-c)**. Large and dense cracks can be seen on the worn surface of PI and PI/fluorographene 1, while smaller microcracks can be seen on the worn surface of PI/FG-0.5. The wear rate and friction coefficient decrease with the addition of 0.5 wt.% of fluorographene to the PI, which is believed to be an optimal amount. Moreover, the water contact angle of PI/fluorographene-0.5 is high compared to pure PI. FG promotes the formation of transfer films during the fracture, enhancing the wear resistance. According to Zhou et al [135]., the coefficient of friction and wear rate of PI/fluorographene can be further reduced by adding CNT to the mixture. Ci et al [136]. reported that the tribological properties of Gas to Liquid (GTL) based oil is enhanced by the addition of fluorographene. Compared to pure oil lubricant, the coefficient of friction, and wear rate decreased by 35% and 90%, respectively, when the concentration of fluorographene was 0.3 $mg \cdot mL^{-1}$. Zhao and Ci [137] reported that the GTL-8 with TiO_2/FGO (1:4) nanocomposite additives of a concentration of 0.3 $mg \cdot mL^{-1}$ exhibits a coefficient of friction and wear rate of 33.67% and 88.38%, respectively, less than pure GTL-8 lubricant, which would mean that the inclusion of TiO_2 to the FG/GTL-8 has no influence on improvising the coefficient of friction and wear rate.

5.3. Gas Sensors

Graphene has been given special attention for gas sensing applications because of the sp^2-hybridized 2D hexagonal honeycomb structure [138,139]. Although graphene can be used as a gas sensing material, functional groups that can stably adsorb gases are not found on the graphene surface. Moreover, graphene-based materials require platinum group metals or oxygen functional groups to enable their gas sensing characteristics [140]. Park et al [141]. reported that the gas sensor fabricated using FGO showed a 7% change in resistive response while sensing NH_3 gas, whereas non-treated GO does not show any response. Katkov et al [142]. proposed backside fluorine-functionalised graphene material as an NH_3 sensor. The graphene layers were recovered by exposing fluorinated HOPG to hydrazine hydrate vapour. The restored sp^2 hybridisation in the reduced fluorinated graphene enhances the

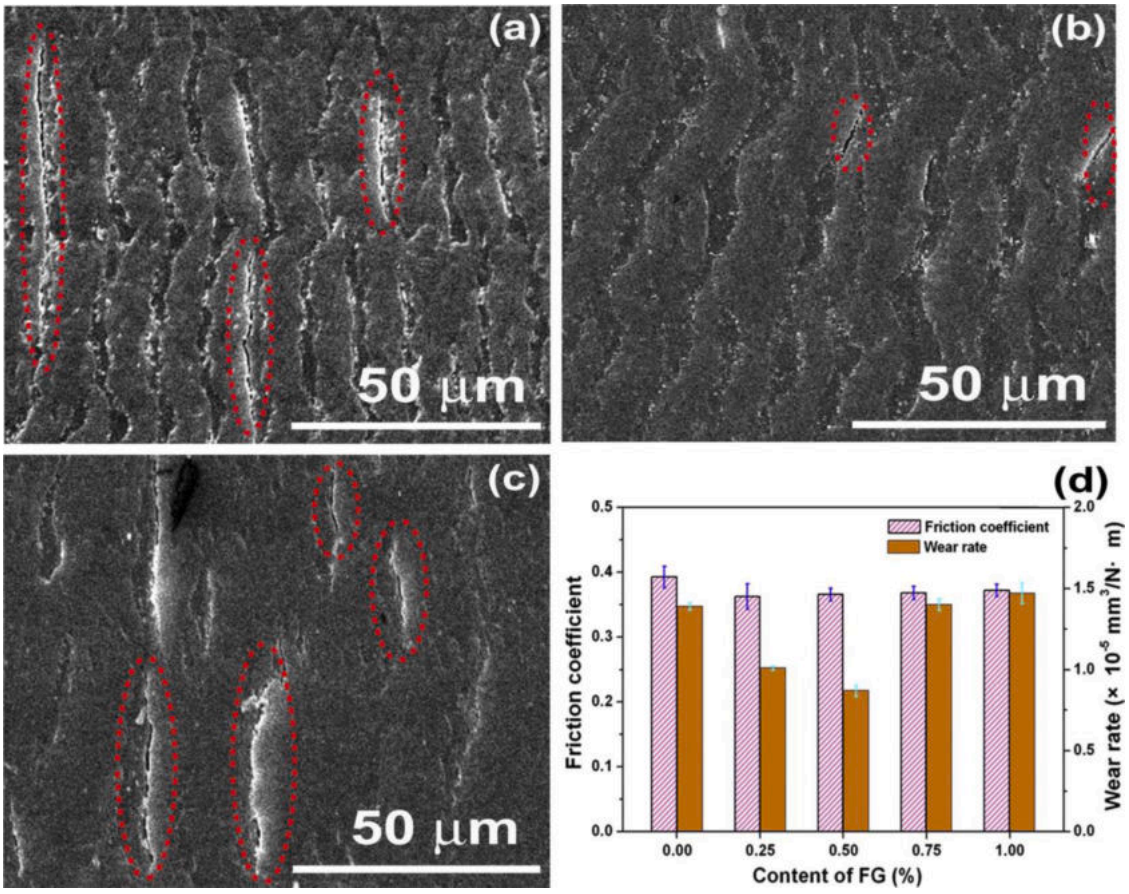

Fig. 10. SEM image of worn surface for the samples of PI (a) PI/fluorographene-0.5 (b) and PI/fluorographene-1 (c); (d) the histogram of friction coefficient and wear rate of all coatings under drying sliding condition. Reproduced with permission [134]. Copyright 2016, Elsevier. (License no. 5177090928007)

material's electrical properties. The residual fluorine atoms that are chemically attached to the graphene attract the NH_3 molecules, acting as sensor zones. The sensor zones are restored to their original state by air purging at RT.

Kang and Li [143] investigated the gas sensitivity of FGO samples towards NH_3 gas, which was prepared by ultrasonic exfoliation of fluorinated graphite. The at.% of C, O and F in FGO were 75.4, 8.79 and 15.81, respectively. The relative response and response time were 9.24% and 87 s, respectively. It was found that the sensitivity of FGO to NH_3 was 3.5 times that of graphene to NH_3 gas. Moreover, the recovery time (time required to reach its initial state) was only 95 s, which is extraordinarily low compared to the recovery time of pristine graphene, which is 7200 s. The first principle studies reveal that FG has weaker interaction towards the adsorbed gas molecules than oxygenated graphene materials, meaning that FG's recovery rate is lower than oxygenated ones [144]. FG spontaneously recovers to its initial state by argon purging, without any additional process like heating or vacuum pumping.

5.4. Other Applications

The applications of FG are widespread as the properties of the material can be controlled by proper F/C tuning. FG can be used as quantum dots [145], as supercapacitors [146] and in bioapplications [147, 148].

Feng et al [145]. synthesised fluorinated graphene quantum dots (F-GQDs) from the thermal cutting of FG F-GQDs with a low F/C ratio (0.03) exhibits excitation wavelength-dependent properties with multicolour photoluminescence (from blue to green). The F-adatoms located at the edge of F-GFDs introduce paramagnetic centres. The F-GQDs show strong paramagnetic behaviour due to the presence of magnetic zigzag edges and sp^3-type defects.

Cao et al [146]. prepared porous partially fluorinated graphene (PFG) by the one-pot hydrothermal method. The C-F semi-covalent bonds can be easily regulated via this method. The symmetric capacitors assembled by PFG exhibit a high specific capacitance of 269.7 $F{\cdot}g^{-1}$ at 1 $A{\cdot}g^{-1}$ with a superior rate capability of 89.3% capacity retention (20 $A{\cdot}g^{-1}$) and a high energy density of 9.4 $Wh{\cdot}kg^{-1}$ at a power density of 250 $W{\cdot}kg^{-1}$.

Jahanshahi et al [147]. studied the bioapplication of FGO, which could be potentially used as nanocarriers to transport the drugs to the affected area in the body. A water-soluble and pH-sensitive charge-reversal FGO was redesigned with polyethyleneimine attached to sericin polypeptide (FPS). The curcumin was loaded to an FPS nanocarrier, where the nanocarrier was characterised for anti-cancer drug delivery. The nanocarrier's design was in such a way that it could selectively enhance cell internalisation and targeted delivery to cancer cell sites. It was also found that the FPS can carry high loads of curcumin, and it could be a promising candidate to be used in chemotherapy. Wang et al [148]. developed hyaluronic acid (HA)-modified fluorinated graphene/Fe_2O_3 composite, which possessed HA and magnetism-induced dual-targeting effect towards cancer cells and high near-infrared adsorption of photothermal therapy. The composite also showed a turnoff fluorescence effect towards anti-cancer drug doxorubicin, which allows monitoring drug loading procedures and chemotherapy. The maximum drug loading ability of the composite of 2.51 mg/mg was achieved.

Very recently, a review on synthesis and application of fluorinated graphene was published [149].

6. Conclusion

The fluorinated carbon materials have a variety of properties, and the properties differ with the change in the type of carbon material fluorinated. In recent times, more attention has been given to graphene and its derivatives, especially F-graphene. The properties of fluorographene are drastically different from the graphene as the graphene lacks π-conjugated electrons, which opens up the material's bandgap, making it an insulator. The F/C ratio and C-F bond characteristics highly depend upon the synthesis method, where exfoliation and direct fluorination are the main methods adopted for FG synthesis. The properties of FG can be controlled through precise tuning of the F/C ratio and maintaining the semi-ionic bonds present in the materials. For instance, increasing the F/C increases the bandgap, which makes the material more insulating. It is well known that the control over the C-F bond characteristics is complex and requires special attention. FG comprises a mixture of ionic, semi-ionic and covalent bonds and a proper screening needs to be done before using the material in energy storage devices and supercapacitors to obtain high efficiency. FG has attractive applications in batteries, supercapacitors, lubrication, bioapplications (especially as drug carriers), quantum dots and sensors. The low surface energy, high thermal stability, chemical inertness and availability make FG an extraordinary material among the 2D materials. Having said that, FG still cannot be completely adapted in primary lithium batteries, as FG is an insulator and its insulating ability increases with an increase in F/C ratio, thus restraining the diffusion of Li^+ ions (resulting in poor discharge rate). The electrochemical properties of FG can be enhanced by introducing dopants and optimizing the F/C ratio. The specific surface area of fluorinated graphene sheets is 400 $m^2 \cdot g^{-1}$, which is well below its theoretical value. Thus limiting the utilisation of FG in its potential applications. The problem can be solved by preparing FG by fluorination of porous graphene, which has a high specific surface area of 1100 $m^2 \cdot g^{-1}$.

Despite the recent progress made in the synthesis of fluorinated graphene, there are shortcomings in both exfoliation and fluorination, as these methods are limited to laboratory scale. Direct gas fluorination can easily be adapted to large-scale production of FG, however, the main dropback is poor controllability of the F/C ratio and C-F bonding character (formation of ionic and semi-ionic C-F bonds). FG synthesised using liquid-phase exfoliation requires further purification, which is time-consuming and contains toxic byproducts. FG prepared using plasma exfoliation contain fluorine radicals on its surface, thus requiring separation before using them in any applications. The lamellar structure of FG prepared using mechanical exfoliation are damaged and FG produced from this technique has a low yield. A chemical process with the ability of selective fluorination to control the C-F bond characteristics and F/C ratio is of primary importance. Significant research should be conducted in designing a defluorination method that could align with the fluorination process. Defluorination can be used in modifying the C-F bonding character and F/C ratio of FG as desired. Other than controllability and homogeneity, the multifunctionality of FG would be of great interest for future research. A proper cost-efficient and environmentally friendly method for industrial-scale manufacturing of FG are yet to be found, and rapid research in this area would undoubtedly enable such a method soon.

Funding

The work is performed as a part of the state assignment for the science of Siberian Federal University, project number FSRZ-2020-0013.

Declaration of Competing Interest

The authors declare no conflict of interest.

Reference

[1] H. Yokomichi, T. Hayashi, A. Masuda, Changes in structure and nature of defects by annealing of fluorinated amorphous carbon thin films with low dielectric constant, Appl. Phys. Lett. 72 (1998) 2704–2706.
[2] Y.S. Lee, Synthesis and properties of fluorinated carbon materials, J. Fluorine Chem. 128 (2007) 392–403.
[3] S. Yuan, M. Rösner, A. Schulz, T.O. Wehling, M.I. Katsnelson, Electric structure and optical properties of partially and fully fluorinated graphene, Phys. Rev. Lett. 114 (2015), 047403.
[4] H. Groult, A. Tressaud, Use of inorganic fluorinated materials in lithium batteries and in energy conversion system, Chem. Commun. 54 (2018) 11375–11382.
[5] Z. Yang, L. Wang, W. Sun, S. Li, T. Zhu, G. Liu, Superhydrophobic poxy coating modified by fluorographene used for anti-corrosion and self-cleaning, Appl. Surf. Sci. 401 (2017) 146–155.
[6] M. Adamska, U. Narkiewicz, Fluorination of carbon nanotubes: A review, J. Fluorine Chem. 200 (2017) 179–189.
[7] H. Sjostrom, S. Stafstrom, M. Boman, J.E. Sundgren, Superhard and elastic carbon nitride thin films having fullerene-like microstructure, Phys. Rev. Lett. 75 (1995) 1336–1339.
[8] S. Kundoo, P. Saha, K. Chattopadhyay, Electron field emission from nitrogen and sulfur-doped diamond-like carbon films deposited by simple electrochemical route, Mater. Lett. 58 (2004) 3920–3924.
[9] R. McCann, S.S. Roy, P. Papakonstantinou, J.A. McLaughlin, S.C. Ray, Spectroscopic analysis of a-C and a-CN_x films prepared by ultrafast high repetition rate pulsed laser deposition, J. Appl. Phys. 97 (2005), 073522.
[10] K. Endo, K. Shinoda, T. Tatsumi, Plasma deposition of low-dielectric-constant fluorinated amorphous Carbon, J. Appl. Phys. 86 (1999) 2739–2745.
[11] H. Touhara, F. Okino, Property control of carbon materials by fluorination, Carbon 38 (2000) 241–267.
[12] S. Agraharam, D.W. Hess, P.A. Kohl, S.A. Bidstrup Allen, Plasma chemistry in fluorocarbon film deposition from pentafluoroethane/argon mixture, J. Vacc. Sci. Tech. B 19 (2001) 439–446.
[13] A. Furlan, G.K. Gueorguiev, H. Högberg, S. Stafström, L. Hultman, Fullerene-like CP_x: A first-principle study of the relative stability of precursors and defect energetics during synthetic growth, Thin Solid Films 515 (2006) 1028–1032.
[14] G.K. Gueorguiev, A. Furlan, H. Högberg, S. Stafström, L. Hultman, First-principles calculations on the structural evolution of solid fullerene-like CP_x, Chem. Phys. Lett. 426 (2006) 374–379.
[15] A. Furlan, G.K. Gueorguiev, Z. Czigány, H. Högberg, S. Braun, S. Stafström, L. Hultman, Synthesis of phosphorus-carbide thin films by magnetron sputtering, Phys. Status Solidi RRL. 2 (2008) 191–193.
[16] C. Goyenola, G.K. Gueorguiev, S. Stafström, L. Hultman, Fullerene-like CSx: A first-principles study of synthetic growth, Chem. Phys. Lett. 506 (2011) 86–91.
[17] C. Goyenola, S. Stafström, L. Hultman, G.K. Gueorguiev, Structural Patterns Arising during Synthetic Growth of Fullerene-Like Sulfocarbide, J. Phys. Chem. C 116 (2012) 21124–21131.
[18] P.F. Fulvio, S.S. Brown, J. Adcock, R.T. Mayes, B. Guo, X. Sun, S.M. Mahurin, G. M. Veith, S. Dai, Low-temperature fluorination of soft-templated mesoporous carbons for a high-power lithium/carbon fluoride battery, Chem. Mater. 23 (2011) 4420–4427.
[19] S. Zhou, S.D. Sherpa, D.W. Hess, A. Bongiorno, Chemical Bonding of Partially Fluorinated Graphene, J. Phys. Chem. C 118 (2014) 26402–26408.
[20] S. Peng, S. Yan, N. Wang, W. Nan, J. Wang, X. Chen, C. Wang, X. Qi, S. Dai, Fluorinated graphene/sulfur hybrid cathode for high energy and high power density lithium primary batteries, RSC Adv 8 (2018) 12701–12707.
[21] J. Giraudet, C. Delabarre, K. Guérin, M. Dubois, F. Masin, A. Hamwi, Comparative performances for primary lithium batteries of some covalent and semi-covalent graphite fluorides, J. Power Sources 158 (2006) 1365–1372.
[22] N. Ariel, M. Eizenberg, Y. Wang, S.P. Murarka, Deposition temperature effect on thermal stability of fluorinated amorphous carbon films utilised as low-K dielectrics, Mater. Sci. Semicond. Process. 4 (2001) 383–391.
[23] H. Biederman, RF sputtering of polymers and its potential application, Vacuum 59 (2000) 594–599.
[24] K.S. Novoselov, A.K. Geim, S.V. Morozov, D. Jiang, Y. Zhang, S.V. Dubonos, I. V. Grigorieva, A.A. Firsov, Electric Field Effect in Atomically Thin Carbon Films, Science 306 (2004) 666–669.
[25] X. Huang, X. Qi, F. Boey, H. Zhang, Graphene-based composites, Chem. Soc. Rev. 41 (2012) 666–686.
[26] J.E. Johns, M.C. Hersam, Atomic Covalent Functionalization of Graphene, Acc. Chem. Res. 46 (2013) 77–86.
[27] M. Khan, M.N. Tahir, S.F. Adil, H.U. Khan, M.R.H. Siddiqui, A.A. Al-warthan, W. Tremel, Graphene based metal and metal oxide nanocomposites: synthesis, properties and their applications, J. Mater. Chem. A 3 (2015) 18753–18808.
[28] Md.S.A. Bhuyan, Md.Nizam Uddin, Md.Maksudul Islam, F.A. Bipasha, S. S. Hossain, Synthesis of graphene, Int. Nano. Lett. 6 (2019) 65–83.
[29] A. Shekhawat, R.O. Ritchie, Toughness and strength of nanocrystalline graphene, Nat. Commun. 7 (2016) 10546.
[30] M.I. Katsnelson, Graphene: Carbon in two dimensions, Mater. Today 10 (2007) 20–27.
[31] M. Tahriri, M. Del Monico, A. Moghanian, M. Tavakkoli Yaraki, R. Torres, A. Yadegari, L. Tayebi, Graphene and its derivatives: Opportunities and challenges in dentistry, Mater. Sci. Eng. C 102 (2019) 171–185.
[32] V. Rosa, H. Xie, N.K. Dubey, T.T. Madanagopal, S.S. Rajan, J.L. Paul Morin, I. Islam, A.H. Castro Neto, Graphene oxide-based substrate: physical and surface

characterisation, cytocompatibility and differentiation potential of dental pulp stem cells, Dent. Mater. 32 (2016) 1019–1025.
[33] N.K. Dubey, R. Bentini, I. Islam, T. Cao, A.H. Castro Neto, V. Rosa, Graphene: A Versatile Carbon-Based Material for Bone Tissue Engineering, Stem Cells Int (2015), 804213, 2015.
[34] W. Gao, In Graphene Oxide, W. Gao, The Chemistry of Graphene Oxide, Springer, Cham., Chapter, 2015, pp. 61–95.
[35] J.T. Robinson, J.S. Burgess, C.E. Junkermeier, S.C. Badescu, T.L. Reinecke, F. K. Perkins, M.K. Zalalutdniov, J.W. Baldwin, J.C. Culbertson, P.E. Sheehan, E. S. Snow, Properties of fluorinated graphene films, Nano Lett 10 (2010) 3001–3005.
[36] O. Ruff, O. Bretschneider, Die Reaktionsprodukte der verschiedenen Kohlenstoffformen mit Fluor II. Kohlenstoff-monofluorid, Z. Anorg. Allg. Chem. 217 (1934) 1–18.
[37] C. Cavallari, M. Brunelli, S. Radescu, M. Dubois, N. Batisse, G.B.M. Vaughan, H. E. Fischer, V. Pischedda, Structural and electronic changes in graphite fluorides as a function of fluorination rate: An XRS, PDF and DFT study, Carbon 147 (2019) 1–8.
[38] A. Hamwi, K. Guerin, M. Dubois, Chapter 17, Fluorine-intercalated graphite for lithium batteries, in: T. Nakajima, H. Groult (Eds.), Fluorinated Materials for Energy Conversion, Elsevier, Amsterdam, 2005, pp. 369–395.
[39] K. Guerin, J.P. Pinheiro, M. Dubois, Z. Fawal, F. Masin, R. Yazami, A. Hamwi, Synthesis and Characterisation of Highly Fluorinated Graphite Containing sp^2 and sp^3 Carbon, Chem. Mater. 16 (2004) 1786–1792.
[40] C. Delabarre, K. Guerin, M. Dubois, J. Giraudet, Z. Fawal, A. Hamwi, Highly fluorinated graphite prepared from graphite fluoride formed using BF_3 catalyst, J. Fluorine. Chem. 126 (2005) 1078–1087.
[41] M. Adamska, U. Narkiewicz, Fluorination of Carbon Nanotubes - A Review, J. Fluorine Chem. 200 (2017) 179–189.
[42] H. Park, J. Zhao, J.P. Lu, Effects of Sidewall Functionalization on Conducting Properties of Single-Wall Carbon Nanotubes, Nano Lett 5 (2006) 916–919.
[43] V.N. Khabashesku, W.E. Billups, J.L. Margrave, Fluorination of Single-Wall Carbon Nanotubes and Subsequent Derivatisation Reactions, Acc. Chem. Res. 35 (2002) 1087–1095.
[44] E.T. Mickelson, C.B. Huffman, A.G. Rinzler, R.E. Smalley, R.H. Hauge, J. L. Margrave, Fluorination of single-wall carbon nanotubes, Chem. Phys. Lett. 296 (1998) 188–194.
[45] T. Nakajima, S. Kasamatsu, Y. Matsuo, Synthesis and characterisation of fluorinated carbon nanotube, Eur. J. Solid State Inorg. Chem. 33 (1996) 831–840.
[46] A. Hamwi, H. Alvergnat, S. Bonnamy, F. Beguin, Fluorination´ of Carbon Nanotubes, Carbon 35 (1997) 723–728.
[47] X. Wang, Y. Chen, Y. Dai, Q. Wang, J. Gao, J. Huang, J. Yang, X. Liu, Preparing Highly Fluorinated Multiwall Carbon Nanotube by Direct Heating-Fluorination during the Elimination of Oxygen-Related Groups, J. Phys. Chem. C 117 (2013) 12078–12085.
[48] A. Felten, C. Bittencourt, J.J. Pireaux, G. Van Lier, J.C. Charlier, Radio-frequency plasma functionalisation of carbon nanotubes surface O_2, NH_3, and CF_4 treatments, J. Appl. Phys. 98 (2005), 074308.
[49] K. Shoda, S. Takeda, Systematic characterisation of carbon nanotubes functionalised in CF_4 plasma, Jpn. J. Appl. Phys. 96 (2007), 216103.
[50] A. Felten, J. Ghijsen, J.J. Pireaux, R.L. Johnson, C.M. Whelan, D. Liang, G. Van Tendeloo, C. Bittencourt, Photoemission study of CF_4 rf-Plasma treated multi-wall carbon nanotubes, Carbon 46 (2008) 1271–1275.
[51] A. Hamwi, C. Latouche, B. Burteaux, J. Dupuis, Preparation and Characterization of Inorganic Fluorides-Fullerenes Compounds, Fullerene Sci. Technol. 4 (1996) 1213–1226.
[52] F. Okino, H. Touhara, K. Seki, R. Mitsumoto, K. Shigematsu, Y. Achiba, Crystal Structure of C60Fx, Fullerene Sci. Technol. 1 (1993) 425–436.
[53] O.V. Boltalina, A.Yu. Lukonin, V.K. Pavlovich, L.N. Sidorov, R. Taylor, A. K. Abdul-Sada, Reaction of [60]fullerene with terbium (IV) fluoride, Fullerene Sci. Technol. 6 (1998) 469–479.
[54] Y. Liu, R.L. Vander Wal, V.N. Khabashesku, Functionalisation of carbon nanoonions by direct fluorination, Chem. Mater. 19 (2007) 778–786.
[55] S. Lousinian, S. Logothetidis, A. Laskarakis, M. Gioti, Haemocompatibility of amorphous hydrogenated carbon thin films, optical properties and adsorption mechanisms of blood plasma proteins, Biomol. Eng. 24 (2007) 107–112.
[56] M. Jiang, Z. Ning, Influence of deposition pressure on the structure and properties of fluorinated diamond-like carbon films prepared by RF reactive magnetron sputtering, Surf. Coat. Technol. 200 (2006) 3682–3686.
[57] T. Hasebe, A. Shimada, T. Suzuki, Y. Matsuoka, T. Saito, S. Yohena, A. Kamijo, N. Shiraga, M. Higuchi, K. Kimura, H. Yoshimura, S. Kuribayashi, Fluorinated diamond-like carbon as antithrombogenic coating for blood-contacting devices, J. Biomed. Mater. Res., Part A 76A (2006) 86–94.
[58] J.C. Sung, M.C. Kan, M. Sung, Fluorinated DLC for tribological applications, Int. J. Refract. Met. Hard Mater. 27 (2009) 421–426.
[59] M.H. Ahmed, J.A. Byrne, J. McLaughlin, Evaluation of glycine adsorption on diamond like Carbon (DLC) and fluorinated DLC deposited by plasma-enhanced chemical vapour deposition (PECVD), Surf. Coat. Technol. 209 (2012) 8–14.
[60] A. Bendavid, P.J. Martin, L. Randeniya, M.S. Amin, The properties of fluorine containing diamond-like carbon films prepared by plasma-enhanced chemical vapour deposition, Diamond Relat. Mater. 18 (2009) 66–71.
[61] W. Feng, P. Long, Y. Feng, Y. Li, Two-dimensional fluorinated graphene: synthesis, structures, properties and applications, Adv. Sci. 3 (2016), 1500413.
[62] P. Gong, Z. Wang, J. Wang. H. Wang, Z. Li, Z. Fan, Y. Xu, X. Han, S. Yang, One-pot sonochemical preparation of fluorographene and selective tuning of its fluorine coverage, J. Mater. Chem. 22 (2012) 16950.
[63] J. Sun, S. Chen, H. Liu, C. Xiong, J. Wang, X. Xie, J. Xue, P. Chen, Z. Nie, Fluorographene nanosheets: a new carbon-based matrix for the detection of small molecules by MALDI-TOF MS, RSC Adv 6 (2016) 99714–99719.
[64] F. Lei, M. Yang, F. Jiang, H. Zhang, Z. Zhang, D. Sun, Microwave-assisted liquid phase exfoliation of graphite fluoride into fluorographene, Chem. Eng. J. 360 (2019) 673–679.
[65] M. Herraiz, M. Dubois, N. Batisse, S. Hajjar-Garreau, L. Simon, Large-scale synthesis of fluorinated graphene by rapid thermal exfoliation of highly fluorinated graphite, Dalton Trans 47 (2018) 4596–4606.
[66] M. Dubois, K. Guerin, Y. Ahmad, N. Batisse, M. Mar, L. Frezet, W. Hourani, J. Bubendorff, J. Parmentier, S. Hajjar-Garreau, L. Simon, Thermal exfoliation of fluorinated graphite, Carbon 77 (2014) 688–704.
[67] V.Mazµnek O.Jankovsky, K. Klímova, D. Sedmidubsky, J. Kosina, M. Pumera, Z. Sofer, Simple synthesis of fluorinated graphene: Thermal exfoliation of fluorographite, Chem. Eur. J. 22 (2016) 17696–17703.
[68] P. Gong, Z. Wang, Z. Fan, W. Hong, Z. Yang, J. Wang, S. Yang, Synthesis of chemically controllable and electrically tunable graphene films by simultaneously fluorinating and reducing graphene oxide, Carbon 72 (2014) 176–184.
[69] H. Aghamohammadi, A. Heidarpour, S. Ghasemib, Electrochemical synthesis of fluorinated graphene nanoplatelets in electrolytes containing hydrofluoric acid and TiO_2 nanoparticles, FlatChem 22 (2020), 100172.
[70] H. Aghamoammadi, M. Bakhtiari, R.E. Farsani, An experimental investigation on the synthesis of fluorographene by electrochemical method in the mixture of sulfuric and hydrofluoric acid electrolytes, Ceram. Int. 46 (2020) 25189–25199.
[71] M.C. Vu, N.A.T. Thieu, J.H. Lim, W.K. Choi, J.C. Won, M.A. Islam, S.R. Kim, Ultrathin thermally conductive yet electrically insulating exfoliated graphene fluoride film for high performance heat dissipation, Carbon 157 (2020) 741–749.
[72] C. Wan, M. Ma, One-step exfoliation and functionalisation of fluorinated graphene sheets from fluoride graphite by ammonia carbonate-assisted solid ball milling, J. Porous Mater. 27 (2020) 1319–1328.
[73] X. Bi, Y. Li, Z. Qiu, C. Liu, T. Zhou, S. Zhuo, J. Zhou, Fluorinated graphene prepared by direct fluorination of n, o-doped graphene aerogel at different temperatures for lithium primary batteries, Materials 11 (2018) 1072.
[74] X. Wang, W. Wang, D. Xu, Y. Liu, W. Lai, X. Liu, Activation effect of porous structure on fluorination of graphene based materials with large specific surface area at mild condition, Carbon 124 (2017) 288–295.
[75] W. Lai, X. Wang, Y. Li, Y. Liu, T. He, K. Fan, X. Liu, The particular phase transformation during graphene fluorination process, Carbon 132 (2018) 271–279.
[76] H. Zhang, L. Fan, H. Dong, P. Zhang, K. Nie, J. Zhong, Y. Li, J. Guo, X. Sun, Spectroscopic Investigation of Plasma-Fluorinated Monolayer Graphene and Application for Gas Sensing, ACS Appl. Mater. Inter. 8 (2016) 8652–8661.
[77] C. Struzzi, M. Scardamaglia, N. Reckinger, H. Sezen, M. Amati, L. Gregoratti, J. F. Colomer, C. Ewels, R. Snyders, C. Bittencourt, Probing plasma fluorinated graphene via Spectromicroscopy, Phys. Chem. Chem. Phys. 19 (2017) 31418–31428.
[78] J. Plsek, K.A. Drogowska, M. Fridrichova, J. Vejpravova, M. Kalbac, Laser-ablation-assisted SF_6 decomposition for extensive and controlled fluorination of graphene, Carbon 145 (2019) 419–425.
[79] R. Yang, L. Zhang, Y. Wang, Z. Shi, D. Shi, H. Gao, E. Wang, G. Zhang, An Anisotropic Etching Effect in the Graphene Basal Plane, Adv. Mater. 22 (2010) 4014–4019.
[80] X. Yu, K. Lin, K. Qiu, H. Cai, X. Li, J. Liu, N. Pan, S. Fu, Y. Luo, X. Wang, Increased chemical enhancement of Raman spectra for molecules adsorbed on fluorinated reduced graphene oxide, Carbon 50 (2012) 4512–4517.
[81] X. Wang, Y. Dai, J. Gao, J. Huang, B. Li, C. Fan, J. Yang, X. Lin, High-yield production of highly fluorinated graphene by direct heating fluorination of graphene-oxide, ACS Appl. Mater. Interfaces 5 (2013) 8294–8299.
[82] P. Meduri, H. Chen, J. Xiao, J.J. Martinez, T. Carlson, J. Zhang, Z.D. Deng, Tunable electrochemical properties of fluorinated graphene, J. Mater. Chem. A 1 (2013) 7866–7869.
[83] Y. Sato, K. Itoh, R. Hagiwara, T. Fukunaga, Y. Ito, On the so-called "semi-ionic'' C–F bond character in fluorine–GIC, Carbon 42 (2004) 3243–3249.
[84] W. Zhang, M. Dubois, K. Guerin, P. Bonnet, H. Kharbache, F. Masin, A. P. Kharitonov, A. Hamwi, Effect of curvature on C–F bonding in fluorinated carbons: from fullerene and derivatives to graphite, Phys. Chem. Chem. Phys. 12 (2010) 1388–1398.
[85] X. Wang, W. Wang, Y. Liu, M. Ren, H. Xiao, X. Liu, Characterisation of conformation and locations of C-F bonds in graphene derivatives by polarised ATR-FTIR, Anal. Chem. 88 (2016) 3926–3934.
[86] P. Gong, Z. Wang, Z. Li, Y. Mi, J. Sun, Y. Niu, H. Wang, J. Wang, S. Yang, Photochemical synthesis of fluorinated graphene via a simultaneous fluorination and reduction route, RSC Adv 3 (2013) 6327–6330.
[87] M. Ren, X. Wang, C. Dong, B. Li, Y. Liu, T. Chen, P. Wu, Z. Cheng, X. Liu, Reduction and transformation of fluorinated graphene induced by ultraviolet irradiation, Phys. Chem. Chem. Phys. 17 (2015) 24056–24062.
[88] Y. Li, X. Wang, W. Wang, R. Qin, W. Lai, A. Ou, Y. Liu, X. Liu, Nitrogen-doping chemical behavior of graphene materials with assistance of defluorination, J. Phys. Chem. C 123 (2019) 584–592.
[89] L. Liao, H. Peng, Z. Liu, Chemistry makes graphene beyond graphene, J. Am. Chem. Soc. 136 (2014) 12194–12200.
[90] D.K. Samarakoon, Z. Chen, C. Nicolas, X. Wang, Structural and electronic properties of fluorographene, Small 7 (2011) 965–969.
[91] K. Jeon, Z. Lee, E. Pollak, L. Moreschini, A. Bostwick, C. Park, R. Mendelsberg, V. Radmilovic, R. Kostecki, T.J. Richardson, E. Rotenberg, Fluorographene: A

Wide Bandgap Semiconductor with Ultraviolet Luminescence, ACS Nano 5 (2011) 1042–1046.
[92] Z. Wang, J. Wang, Z. Li, P. Gong, X. Liu, L. Zhang, J. Ren, H. Wang, S. Yang, Synthesis of fluorinated graphene with tunable degree of fluorination, Carbon 50 (2012) 5403–5410.
[93] V. Kumar, R. Santosh, First-principle calculations of structural, electronic, optical and thermodynamical properties of fluorinated graphene, Mater. Sci. Eng. B 246 (2019) 127–135.
[94] M.M. Khatami, G. Gaddemane, M.L. Van de Put, M.K. Moravvej-Farshi, W. G. Vandenberghe, Electronic transport properties of hydrogenated and fluorinated graphene: a computational study, J. Phys. Condens. Matter 32 (2020), 495502.
[95] R.D. Yamaletdinov, V.L. Katkov, Y.A. Nikiforov, A.V. Okotrub, V.A. Osipov, Effect of fluorine patterns on electronic transport in fluorinated graphene, Adv. Theory Simul. 3 (2020), 1900199.
[96] R.R. Nair, W. Ren, R. Jalil, I. Riaz, V.G. Kravets, L. Britnell, P. Blake, F. Schedin, A.S. Mayorov, S. Yuan, M.I. Katsnelson, H.M. Cheng, W. Strupinski, L. G. Bulusheva, O.V. Okotrub, I.V. Grigorieva, A.V. Grigorenko, K.S. Novoselov, A. K. Geim, Fluorographene: A two-dimensional counterpart of Teflon, Small 6 (2010) 2877–2884.
[97] A.A. Mubarak, A.I. Ismail, The effect of substituting an X (B, N, O and F) atom on the structural, magnetic and optical properties of graphene sheets, J. Electron. Mater. 49 (2020) 3225–3233.
[98] M. Sepioni, R.R. Nair, S. Rablen, J. Narayanan, F. Tuna, R. Winpenny, A.K. Geim, I.V. Grigorieva, Limits of intrinsic magnetism in graphene, Phys. Rev. Lett. 105 (2010), 207205.
[99] C.N.R. Rao, H.S.S. Ramakrishna Matte, K.S. Subrahmanyam, U. Maitra, Unusual magnetic properties of graphene and related materials, Chem. Sci. 3 (2012) 45–52.
[100] R.R. Nair, M. Sepioni, I-Ling. Tsai, O. Lehtinen, J. Keinonen, A.V. Krasheninnikov, T. Thomson, A.K. Geim, I.V. Grigorieva, Spin-half paramagnetism in graphene induced by points defects, Nat. Phys. 8 (2012) 199–202.
[101] Q. Feng, N. Tang, F. Liu, Q. Cao, W. Zheng, W. Ren, X. Wan, Y. Du, Obtaining high localised spin magnetic moments by fluorination of reduced graphene oxide, ACS Nano 7 (2013) 6729–6734.
[102] M. Wang, C.M. Li, Investigation of doping effects on magnetic properties of the hydrogenated and fluorinated graphene structures by extra charge mimic, Phys. Chem. Chem. Phys. 15 (2013) 3786–3792.
[103] Q. Feng, Y. Zheng, J. Li, L. Jiang, Y. Lin, Q. Ye, L. Chen, Z. Huang, Observation of ferromagnetic ordering by fragmenting fluorine clusters in highly fluorinated graphene, Carbon 132 (2018) 691–697.
[104] Z.J. Fan, W. Kai, J. Yan, T. Wei, L.J. Zhi, J. Feng, Y.M. Ren, L.P. Song, F. Wei, Facile synthesis of graphene nanosheets via Fe reduction of exfoliated graphite oxide, ACS Nano 5 (2011) 191–198.
[105] F. Withers, T.H. Bointon, M. Dubois, S. Russo, M.F. Craciun, Nanopatterning of fluorinated graphene by electron beam irradiation, Nano Lett 11 (2011) 3912–3916.
[106] K. Tahara, T. Iwasaki, S. Furuyama, A. Matsutani, M. Hatano, Asymmetric transport property of fluorinated graphene, Phys. Lett. 103 (2013), 143106.
[107] M. Kolesnik-Gray, V.I. Sysoev, V.I. Gollwitzer, D.V. Pinakov, G.N. Chekhova, L. G. Bulusheva, O.V. Okotrub, V Krstic, Electrical transport in devices based on edge-fluorinated graphene, Adv. Electron. Mater. 4 (2018), 1800073.
[108] M. Seredych, O. Mabayoye, M. Kolesnik, V. Krstic, T.J. Bandosz, Zinc (hydr) oxide/graphite based-phase composites: effect of the carbonaceous phase on surface properties and enhancement in electrical conductivity, J. Mater. Chem. 22 (2012) 7970–7978.
[109] A.A. Balandin, Thermal properties of graphene and nanostructured carbon materials, Nat. Mater. 10 (2011) 569–581.
[110] L. Peng, Z. Xu, Z. Liu, Y. Guo, P. Li, C. Gao, Ultrahigh thermal conductive yet superflexible graphene films, Adv. Mater. 29 (2017), 1700589.
[111] X. Wang, P. Wu, Highly thermally conductive fluorinated graphene films with superior electrical insulation and mechanical flexibility, ACS Appl. Mater. Inter. 11 (2019) 21946–21954.
[112] W. Huang, Q. Pei, Z. Liu, Y. Zhang, Thermal conductivity of fluorinated graphene: A non-equilibrium molecular dynamics study, Chem. Phys. Lett. 552 (2012) 97–101.
[113] J.J. Hu, S.H. Jo, Z.F. Ren, A.A. Voevodin, J.S. Zabinski, Tribological behavior and graphitisation of carbon nanotubes grown on 440C stainless steel, Tribol. Lett. 19 (2005) 119–125.
[114] D. Berman, A. Erdemir, A.V. Sumant, Graphene: a new emerging lubricant, Mater. Today 17 (2014) 31–42.
[115] K. Hou, P. Gong, J. Wang, Z. Yang, Z. Wang, S. Yang, Structural and tribological characterisation of fluorinated graphene with various fluorine contents prepared by liquid-phase exfoliation, RSC Adv 100 (2014) 56543–56551.
[116] L.F. Wang, T.B. Ma, Y.Z. Hu, H. Wang, T.M. Shao, Ab initio study of the friction mechanism of fluorographene and graphene, J. Phys. Chem. C 117 (2013) 12520–12525.
[117] T. Lim, S. Ju, Control of graphene surface wettability by using CF_4 plasma, Surf. Coat. Technol. 328 (2017) 89–93.
[118] T. Bharathidasan, T.N. Narayanan, S. Sathyanaryanan, S.S. Sreejakumari, Above 170° water contact angle and oleophobicity of fluorinated graphene oxide based transparent polymeric films, Carbon 84 (2015) 207–213.
[119] A. Taqieddin, M. Heiranian, N.R. Aluru, Interfacial properties of water on hydrogenated and fluorinated graphene surfaces: parametrisation of nonbonded interactions, J. Phys. Chem. C 124 (2020) 21467–21475.
[120] S. Kwon, J.H. Ko, K.J. Jeon, Y.H. Kim, J.Y. Park, Enhanced Nanoscale Friction on Fluorinated Graphene, Nano Lett 12 (2012) 6043–6048.
[121] K. Fan, X. Chen, X. Wang, X. Liu, W. Lai, X. Liu, Toward excellent tribological performance as oil-based lubricant additive: Particular tribological behavior of fluorinated graphene, ACS Appl. Mater. Inter. 10 (2018) 28828–28838.
[122] N. Watanabe, M. Fukuda, Primary cell for electric batteries. U.S. Patent 3,536,532, Oct 27, 1970.
[123] N. Watanabe, M. Fukuda, High energy density battery. U.S. Patent 3,700,502, Oct 24, 1972.
[124] D. Damien, P.M. Sudeep, T.N. Narayanan, M.R. Anantharaman, P.M. Ajayan, M. M. Shaijumon, Fluorinated graphene based electrodes for high performance primary lithium batteries, RSC Adv 3 (2013) 25702–25706.
[125] G. Zhong, H. Chen, X. Huang, H. Yue, C. Lu, High-power-density, high-energy-density fluorinated graphene for primary lithium batteries, Front. Chem. 6 (2018) 50.
[126] C. Sun, Y. Feng, Y. Li, C. Qin, Q. Zhang, W. Feng, Solvothermally exfoliated fluorographene for high–performance lithium primary batteries, Nanoscale 6 (2014) 2634–2641.
[127] Z. Luo, X. Wang, D. Chen, Q. Chang, S. Xie, Z. Ma, W. Lei, J. Pan, Y. Pan, J. Huang, Ultrafast Li/Fluorinated Graphene Primary Batteries with High Energy Density and Power Density, ACS Appl. Mater. Inter. 3 (2021) 18809–18820.
[128] I.Y. Jeon, M.J. Ju, J. Xu, H.J. Choi, J.M. Seo, M.J. Kim, I.T. Choi, H.M. Kim, J. C. Kim, J.J. Lee, H.K. Liu, H.K. Kim, S. Dou, L. Dai, J.B. Baek, Edge-fluorinated graphene nanoplatelets as high performance electrodes for dye-sensitised solar cells and lithium ion batteries, Adv. Funct. Mater. 25 (2015) 1170–1179.
[129] S. Chen, F. Zheng, J. Feng, H. Dong, Y. Li, Theoretical study on single-sided fluorinated graphene for lithium storage, Appl. Surf. Sci. 560 (2021), 150033.
[130] W. Liu, R. Guo, Y. Wang, G. Dang, Y. Li, Y. Sun, P. Huang, H. Pei, J. Lu, J. Xie, A low-overpotential sodium/fluorinated graphene battery based on silver nanoparticles as catalyst, J. Colloid Inter. Sci. 565 (2020) 70–76.
[131] H.D. Huang, J.P. Tu, L.P. Gan, C.Z. Li, An investigation on tribological properties of graphite nanosheets as oil additive, Wear 261 (2006) 140–144.
[132] J.S. Lin, L.W. Wang, G.H. Chen, Modification of Graphene Platelets and Their Tribological Properties as a Lubricant Additive, Tribol. Lett. 41 (2011) 209–215.
[133] C. Lee, X. Wei, J.W. Kysar, J. Hone, Measurement of the elastic properties and intrinsic strength of monolayer graphene, Science 321 (2008) 385–388.
[134] X. Ye, X. Liu, Z. Yang, Z. Wang, H. Wang, J. Wang, S. Yang, Tribological properties of fluorinated graphene reinforced polyimide composite coatings under different lubricated conditions, Composites: Part A 81 (2016) 282–288.
[135] S. Zhou, W. Li, W. Zhao, Q. Li, C. Liu, Z. Fang, X. Gao, Tribological behaviors of polyimide composite coatings containing carbon nanotubes and fluorinated graphene with hybrid phase or blend phase, Prog. Org. Coat. 147 (2020), 105800.
[136] X. Ci, W. Zhao, J. Luo, Y. Wu, T. Ge, L. Shen, X. Gao, Z. Fang, Revealing the lubrication mechanism of fluorographene nanosheets enhanced GTL-8 based nanolubricant oil, Tribo. Inter. 138 (2019) 174–183.
[137] W. Zhao, X. Ci, TiO_2 nanoparticle/fluorinated reduced graphene oxide nanosheet composites for lubrication and wear resistance, ACS Appl. Nano Mater. 3 (2020) 8732–8741.
[138] M. Gautam, A.H. Jayatissa, Graphene based field effect transistor for the detection of ammonia, Appl. Phys. Lett. 112 (2012), 064304.
[139] A. Pourjavadi, Z.M. Tehrani, S. Jokar, Functionalised mesoporous silica-coated magnetic graphene oxide by polyglycerol-g-polycaprolactone with pH-responsive behavior: designed for targeted and controlled doxorubicin delivery, J. Ind. Eng. Chem. 28 (2015) 45–53.
[140] J. Wang, B. Singh, J.H. Park, S. Rathi, I. Lee, S. Maeng, H.I. Joh, C.H. Lee, G. H. Kim, Dielectrophoresis of graphene oxide nanostructures for hydrogen gas sensor at RT, Sens. Actuators B 194 (2014) 296–302.
[141] M.S. Park, K.H. Kim, M.J. Kim, Y.S. Lee, NH_3 gas sensing properties of a gas sensor based on fluorinated graphene oxide, Colloids Surf. A 490 (2016) 104–109.
[142] M.V. Katkov, V.I. Sysoev, A.V. Guselnikov, I.P. Asanov, L.G. Bulusheva, A. V. Okotrub, A backside fluorine-functionalised graphene layer for ammonia detection, Phys. Chem. Chem. Phys. 17 (2015) 444–450.
[143] W. Kang, S. Li, Preparation of fluorinated graphene to study its gas sensitivity, RSC Adv 8 (2018) 23459–23467.
[144] V. Sysoev, A.V. Okotrub, I.P. Asanov, P.N. Gevko, L.G. Bulusheva, Advantage of graphene fluorination instead of oxygenation for restorable adsorption of gaseous ammonia and nitrogen dioxide, Carbon 118 (2017) 225–232.
[145] Q. Feng, W. Xiao, Y. Liu, Y. Zheng, Y. Lin, J. Li, Q. Ye, Z. Huang, Novel synthesis of slightly fluorinated graphene quantum dots with luminescent and paramagnetic properties through thermal cutting of fluorinated graphene, Materials 11 (2018) 91.
[146] N. Cao, T. Wang, R. Boukherroub, Y. Cai, Y. Qin, F. Li, P. Liu, Q. Shao, M. Liu, X. Zang, Facile and secure synthesis of porous partially fluorinated graphene employing weakly coordinating anion for enhanced high-performance symmetric supercapacitor, J. Materiomics 8 (2022) 113–122, https://doi.org/10.1016/j.jmat.2021.04.012.
[147] M. Jahanshahi, E. Kowsari, V. Haddadi-Asl, M. Khoobi, J.H. Lee, F.B. Kadumudi, S. Talebian, N. Kamaly, M. Mehrali, Sericin grafted multifunctional curcumin loaded fluorinated graphene oxide nanomedicines with charge switching properties for effective cancer cell targeting, Int. J. Pharm. 572 (2019), 118791.
[148] D. Wang, Y. Zhang, M. Zhai, Y. Huang, H. Li, X. Liu, P. Gong, Z. Liu, J. You, Fluorescence turn-off magnetic fluorinated graphene composite with high nir absorption for targeted drug delivery, Chem. Nano. Mat. 7 (2021) 71–77.
[149] X. Chen, K. Fan, Y. Liu, Y. Li, X. Liu, W. Feng, X. Wang, Recent advances in fluorinated graphene from synthesis to applications: critical review on functional chemistry and structure engineering, Adv. Mater. 34 (2022), 2101665.